Hydrodynamics of Vegetated Channels

Heidi M. Nepf
Department of Civil and Environmental Engineering
Massachusetts Institute of Technology
Cambridge, MA 02139, USA
hmnepf@mit.edu

Running Title: Vegetated Channels

Corresponding Author: Heidi M. Nepf
Department of Civil and Environmental Engineering
Massachusetts Institute of Technology
77 Massachusetts Avenue
Building 48-216D
Cambridge, MA 02139, USA
hmnepf@mit.edu
(617)-253-8622

Abstract:

This paper is a review of some recent studies in vegetation hydrodynamics, focusing on conditions within channels and spanning spatial scales from individual blades, to meadows, to the channel reach. At the blade-scale, the boundary layer formed on the plant surface plays a role in controlling nutrient uptake. Also, flow resistance and light availability are influenced by the reconfiguration of flexible blades. At the meadow-scale there are two flow regimes. For sparse meadows, the flow resembles a rough boundary layer. For dense meadows, the flow resembles a mixing layer. At the reach-scale, flow resistance is more closely connected to patch-scale vegetation distribution, described by the blockage factor, than to the geometry of individual plants. The impact of vegetation distribution on sediment movement is also discussed, with attention given to methods for estimating bed stress within regions of vegetation. To conclude, three examples are given to show how vegetation hydrodynamics plays an important role in the management of environmental systems; in channel restoration, flood management, and carbon cycling.

Introduction

Aquatic vegetation provides a wide range of ecosystem services. The uptake of nutrients and production of oxygen improves water quality (*e.g.* Chambers and Prepas 1994, Wilcock et al. 1999). The potential removal of nitrogen and phosphorous is so high that some researchers advocate widespread planting in waterways (Mars et al. 1999). Seagrasses are essential primary producers, forming the foundation of many food webs (Green & Short 2003), and in river channels vegetation promotes biodiversity by creating different habitat with spatial heterogeneity in the stream velocity (*e.g.* Kemp et al. 2000). Marshes and mangroves reduced coastal erosion by damping waves and storm surge (*e.g.* Brampton 1992, Turker et al. 2006, Othman 1994), and riparian vegetation enhances bank stability (Pollen and Simon 2005). Through the processes described above, aquatic vegetation provides ecosystem services with an estimated annual value of over ten trillion dollars (Costanza et al. 1997). These services are all influenced in some way by the flow field existing within and around the vegetated region.

In rivers, aquatic vegetation was historically considered only as a source of flow resistance, and vegetation was frequently removed to enhance flow conveyance and reduce flooding. Because of this context, the earliest studies of vegetation hydrodynamics focused on the characterization of flow resistance with a strictly hydraulic perspective (*e.g.* Ree 1949, Kouwen and Unny 1973, Kouwen 1990). However, as noted above, vegetation also provides ecological services that make it an integral part of coastal and river systems. To better understand and protect these systems, the study of vegetation hydrodynamics has, over time, become interwoven with other disciplines, such as biology (*e.g.* Hurd 2000, Koch 2001, Huang et al. 2011), fluvial geomorphology (e.g. Bennett et al. 2002, Tal and Paola 2007), landscape ecology (e.g. Larsen and Harvey 2011), and geochemistry (e.g. Clarke 2002, Harvey et al. 2003). This integration will surely accelerate in the future, as our

discipline contributes to understanding and managing environmental systems.

The presence of vegetation alters the velocity field across several scales, ranging from individual branches and blades on a single plant, to the community of plants in a long meadow or finite length patch. Flow structure at the different scales is relevant to different processes. For example, the uptake of nutrients by an individual blade depends on the boundary layer on that blade, *i.e*. on the blade-scale flow (*e.g*. Koch 1994). Similarly, the capture of pollen is mediated by the flow structure generated around individual stigma (*e.g*. Ackerman 1997). In contrast, the retention or release of organic matter, mineral sediments, seeds, and pollen from a meadow of patch depends on the flow structure at the meadow- or patch-scale (*e.g*. Gaylord et al. 2004, Zong and Nepf 2010). Further, spatial heterogeneity in the meadow-scale parameters can lead to complex flow patterns. For example, in a marsh or wetland a branching network of channels cuts through regions of dense, largely emergent vegetation. While the channels provide most of the flow conveyance, the vegetated regions provide most of the ecosystem function and particle trapping. Thus, to describe marsh function one must describe the transport into and circulation within the vegetated regions. These examples tell us that to properly describe the physical role of vegetation within an environmental system, one must first identify the spatial scale relevant to a particular process, and choose models and measurements that are consistent with that scale. The following sections review some fundamental aspects of flow structure at the blade and meadow scale.

2. Flow at the scale of individual blades

2.1 Blade Boundary Layers and Nutrient Fluxes

At the scale of individual blades and leaves, the hydrodynamic response is dominated by boundary layer formation on the plant surface. A flat plate has often been used as a model for flow adjacent to

79 blades and leaves oriented in the streamwise (x) direction (Figure 1). A viscous boundary layer
80 forms at the leading edge ($x = 0$) of the blade, and its thickness, δ, grows with streamwise distance,
81 specifically, $\delta(x) = 5\sqrt{\nu x/U}$, with U the mean current and ν the kinematic viscosity (*e.g.* White
82 2008). As the viscous boundary layer grows thicker, it becomes sensitive to perturbations caused by
83 turbulent oscillations in the outer flow or by irregularities in surface texture. At some point along
84 the blade the boundary layer transitions to a turbulent boundary layer with a viscous sub-layer, δ_s
85 (Figure 1). The transition occurs near $Re_x = Ux/\nu \approx 10^5$, but can be modified by surface roughness
86 (White, 2008). If the length of the blade is less than the transition length, $x_t = 10^5 \nu/U$, the boundary
87 layer is laminar over the entire blade. If the boundary layer becomes turbulent, the viscous sub-layer
88 will have a constant thickness set by the friction velocity on the blade, u_{b*}. Experiments and scaling
89 indicate that the viscous sub-layer is between $\delta_s = 5\nu/u_{b*}$ and $10\nu/u_{b*}$ (*e.g.* Kundu and Cohen 2002,
90 Boudreau and Jorgensen 2001). Within this layer the flow is essentially laminar.

91 Because of the difference in molecular diffusivity, the concentration boundary layer, δ_c, is
92 smaller than the momentum boundary layer, δ_s. Specifically, $\delta_c = \delta_s\, Sc^{-1/3}$, with Schmidt number S_c
93 $= \nu/D_m$ and molecular diffusivity D_m (*e.g.* Boudreau and Jorgensen 2001). The kinematic viscosity
94 of water is of the order $\nu = 10^{-6}$ m^{2}s^{-1} and for most dissolved species D_m is of the order 10^{-9} m^{2}s^{-1}, so
95 that, in water we generally find $\delta_c = 0.1\ \delta_s$. Within δ_c transport perpendicular to the surface can only
96 occur through molecular diffusion, so that this layer is also called the diffusive sub-layer.

97 The mass flux at the surface, $\dot{m}$, is described by Fick's Law (*e.g.* Kays and Crawford, 1993).

98 $$\frac{\dot{m}}{A} = -D_m \frac{\partial C}{\partial n_\perp} \qquad (1)$$

99 Here, A is the surface area, and $\partial C/\partial n_\perp$ is the gradient in concentration perpendicular to the surface.
100 It is often assumed that the flux across δ_c is the rate-limiting step in transferring dissolved species to

101 the blade surface. In this case, the concentration at the surface is assumed to be zero, *i.e*. the plant is
102 a perfect absorber, taking in each molecule the instant it reaches the surface. In addition, because
103 transport across the sub-layer proceeds at the rate of molecular diffusion, it is several orders of
104 magnitude slower than the turbulent diffusion occurring outside this layer. Therefore, it is
105 reasonable to assume that the concentration at the outer edge of the sub-layer is the bulk fluid
106 concentration C. Then, $\partial C/\partial n_{\perp} \approx C/\delta_c$, and (1) can be reduced to (*e.g*. Boudreau and Jorgensen
107 2001),
108
109 $$\dot{m} = \frac{D_m AC}{\delta_c} = \frac{u_*}{10\nu} Sc^{1/3} D_m AC \sim U\,, \tag{2}$$
110
111 where we have used the relations for δ_c introduced above. Equation (2) suggests that the uptake rate
112 increases with increasing velocity, U. Several studies have captured this behavior for nutrient uptake
113 by seagrasses (*e.g.* Koch 1994, Thomas et al. 2000). However, as the velocity increases, at some
114 point the physical rate of mass flux matches and then surpasses the biological rate of incorporation at
115 the blade surface. At this point the uptake rate is controlled biologically, and this is called the
116 biologically-limited flux rate. This transition was observed to occur around $U = 8$ *cm/s* for
117 *Macrocystis integrifolia* blades (Hurd et al. 1996), and around $U = 4$ and *6* cm/s for *Thalassia*
118 *testudinum* and *Cymodocea nodosa*, respectively (Koch 1994). The transition velocity depends on
119 the biological rate, which in turn depends on light availability and temperature (Koch 1994).
120 A flat plate is not always a good geometric model for a plant surface. However, a
121 generalized version of (2) will hold for surfaces of any shape or rigidity, and mass-transport
122 limitation by a diffusive sub-layer can occur on any surface. Specifically, the mass-flux can be
123 described at any point on the surface by $\dot{m} = D_m AC/\delta_c$. The problem lies in describing the sub-layer

thickness, δ_c, which can vary along the surface due to changes in surface texture, and due to the surface shape. For example, on an undulated blade of the kelp *Macrocystis integrifolia*, the laminar sub-layer is thinned at the apex of each undulation, and thickened on the downstream side, relative to a flat blade under the same mean flow conditions (Hurd et al. 1997). Further, blade motion may disturb the diffusive sub-layer, replacing the fluid next the surface with fluid from outside the boundary layer, which in turn creates an instantaneously higher concentration gradient at the surface and thus higher fluxes (*e.g*. Koehl and Alberte 1988, Hurd 2000, Denny and Roberson 2002). This process can be represented by the surface renewal model (Stevens et al. 2003, Huang et al. 2011). Recent studies have documented blade motions associated with turbulence (Plew *et al*. 2008, Siniscalchi e*t al*. 2012), and future studies should examine how the turbulence-induced motion may enhance flux.

2.2 Flexibility and Reconfiguration

Because many aquatic plants are flexible, they can be pushed over by currents, resulting in a change in morphology called reconfiguration (*e.g*. Vogel, 1994). The change in blade posture can alter light availability in two competing ways. When a blade is pushed over, its horizontal projected area increases, creating a larger surface area for light interception, but the greater horizontal projection also increases shading among neighboring bladesm which would tend to reduce light interception (Zimmerman 2003). Reconfiguration also reduces flow resistance through two mechanisms. First, reconfiguration reduces the frontal area of the vegetation, and second, the reconfigured shape tends to be more streamlined (de Langre 2008). Because of reconfiguration, the drag on a plant increases more slowly with velocity, than predicted by the quadratic law. To quantify this deviation from the quadratic law, the relationship between the drag force (F) and

147 velocity (U) has been expressed as $F \propto U^{2+\gamma}$, with γ called the Vogel exponent. The Vogel
148 exponent has been observed to vary between $\gamma = 0$ (rigid) and γ =-2 (very flexible) for aquatic
149 species (Vogel, 1994).

150 In practice, predictions of drag have used the standard quadratic law, but allow the reference
151 area and drag coefficient to vary with velocity. There has been significant debate about which
152 reference area (*e.g*. frontal area) best characterizes drag as the vegetation is pushed over (see
153 discussion of Sand-Jensen 2003 by Green 2005a; Sukhodolov 2005; Statzner et al. 2006). Some
154 recent studies have addressed this debate by developing drag relationships that incorporate the
155 change in posture (*e.g.* Luhar and Nepf 2011).

156 A flexible body in flow will adjust its shape until there is a balance between the drag force
157 and the restoring force due to body stiffness, for which scaling predicts $F \propto U^{4/3}$ (*e.g*. Alben et al.
158 2002, Gosselin et al. 2010, de Langre 2008). Because many aquatic species have gas-filled sacs or
159 material density less than water, buoyancy may also act as a restoring force. Green (2005) and
160 Abdelrhman (2007) developed models for plant posture that consider only buoyancy. Dijkstra and
161 Uittenbogaard (2010) and Luhar and Nepf (2011) considered both buoyancy and rigidity, in which
162 case reconfiguration depends on two dimensionless parameters that represent the ratios of forces
163 associated with drag, rigidity and buoyancy. The Cauchy number, *Ca*, is the ratio of drag and the
164 stiffness restoring force. The buoyancy parameter, *B*, is the ratio of the restoring forces due to
165 buoyancy and stiffness. For a blade of length l, width b, thickness t, and density, ρ_v, and in a
166 uniform flow of horizontal velocity U, these parameters are defined as:
167

168 $$B = \frac{(\rho - \rho_v) g b t l^3}{EI} \qquad (3)$$

169 $$Ca = \frac{1}{2}\frac{\rho C_D b U^2 l^3}{EI} \quad (4)$$

170

171 Here, E is the elastic modulus for the blade, $I(=bt^3/12)$ is the second moment of area, ρ is the density
172 of water, and g is the acceleration due to gravity.

173 As an alternative to empirically determined drag coefficients, $C_D = f(U)$, Luhar and Nepf
174 (2011) proposed an effective blade length, l_e, to describe the impact of reconfiguration on drag. The
175 effective blade length is defined as the length of a rigid, vertical blade that generates the same
176 horizontal drag as the flexible blade of total length l. Based on this definition, the horizontal drag
177 force on the blade is $F_x = (1/2)\rho C_D b l_e U^2$, where the drag coefficient, C_D, for the flexible blades is
178 identical to that for rigid, vertical blades. The following relationships for effective length, l_e, and
179 meadow height, h, are based on the model described in Luhar and Nepf (2011, 2012).

180

181 $$\frac{l_e}{l} = 1 - \frac{1 - 0.9Ca^{-1/3}}{1 + Ca^{-3/2}(8 + B^{3/2})} \quad (5)$$

182 $$\frac{h}{l} = 1 - \frac{1 - Ca^{-1/4}}{1 + Ca^{-3/5}\left(4 + B^{3/5}\right) + Ca^{-2}\left(8 + B^2\right)} \quad (6)$$

183

184 When rigidity is the dominant restoring force ($Ca >> B$), (6) reduces to $h/l \sim Ca^{-1/4} \sim (EI/U^2)^{1/4}$,
185 which is similar to the scaling suggested by Kouwen and Unny (1973) and later by Velasco et al.
186 (2003). Although (5) and (6) were developed for individual blades, Luhar and Nepf (2012)
187 demonstrate how they can be used to predict the height (h) of a submerged meadow, and how the
188 predicted h and l_e can then be used to predict channel-scale resistance.

189

3. Uniform Meadows of Submerged Vegetation

In this section we consider a community of individual plants within a uniform, submerged meadow. The flow at the meadow scale is less dependent on the specific morphology of each plant or blade, but responds instead to the average flow resistance associated with the distribution of meadow elements. The meadow geometry is defined by the scale of individual stems and blades, and the number of these elements per bed area. If the individual stems or blades have a characteristic diameter or width d, and an average spacing ΔS, then the frontal area per volume within the meadow is $a = d/\Delta S^2$. Note that a can only be properly defined as an average of a length-scale greater than ΔS, and by using this representation for meadow geometry we forfeit the resolution of flow structure at scales less than ΔS. The meadow density can also be described by the solid volume fraction occupied by the canopy elements, ϕ, or the porosity, $n = (1-\phi)$. If the individual elements approximate a circular cylinder, *e.g.* reed stems, then $\phi = (\pi/4)\, ad$. If the morphology is strap-like, with blade width d and thickness b, then $\phi = db/\Delta S^2 = ab$. Note that d and ΔS, and therefore a, can vary spatially within the meadow, and specifically over the height of the meadow. In addition, for flexible vegetation, the posture of the blades is influenced by the flow (see discussion in 2.1). As flow speed increases, individual blades are pushed over into more streamlined positions. As the meadow becomes more compressed (decreased meadow height) with increasing flow speed, both a and ϕ increase. Finally, a non-dimensional measure of the canopy density is the frontal area per bed area, λ, known as the roughness density (Wooding, Bradley & Marshall 1973). For meadow height h, and $z = 0$ at the bed,

$$\lambda = \int_{z=0}^{h} a\,dz = ah \tag{7}$$

213 with the right-most expression valid for vertically uniform *a*.

214 Within a canopy, flow is forced to move around each branch or blade, so that the velocity
215 field is spatially heterogeneous at the scale of these elements. A double-averaging method is used to
216 remove the element-scale spatial heterogeneity, in addition to the more common temporal averaging
217 (Gray & Lee 1977; Raupach & Shaw 1982, Nikora 2007 and references therein). The velocity
218 vector $\vec{u} = (u,v,w)$ corresponds to the coordinates (*x, y, z*), respectively. The instantaneous velocity
219 and pressure (*p*) fields are first decomposed into a time average (overbar) and deviations from the
220 time-average (single prime). The time-averaged quantities are further decomposed into a spatial
221 mean (angle bracket) and deviations from the spatial mean (double prime). The spatial averaging
222 volume is thin in the vertical, to preserve vertical variation in meadow density, and large enough in
223 the horizontal plane to include several stems ($> \Delta S$).

224 Applying this averaging scheme to a homogeneous canopy, the momentum equation in the
225 stream-wise direction is (*e.g*. Nikora et al. 2007).

226
$$\frac{D\langle\overline{u}\rangle}{Dt} = g\sin\theta - \frac{1}{n\rho}\frac{\partial n\langle\overline{p}\rangle}{\partial x} - \underbrace{\frac{1}{n}\frac{\partial}{\partial z}n\left\langle\overline{u'w'}\right\rangle}_{\text{(i)}} - \underbrace{\frac{1}{n}\frac{\partial}{\partial z}n\langle\overline{u}''\overline{w}''\rangle}_{\text{(ii)}} + \underbrace{\frac{1}{n}\nu\frac{\partial}{\partial z}n\frac{\partial\langle\overline{u}\rangle}{\partial z}}_{\text{(iii)}} - D_x \qquad (8)$$

227 Here, θ is the bed slope. Term (i) is the spatial-average of the Reynolds' stress. Term (ii), called the
228 dispersive stress, is the momentum flux associated with spatial correlations in the time-averaged
229 velocity field. Poggi et al. (2004b) show that the dispersive stress is less than 10% of the Reynolds
230 stress (i) for $\lambda = ah > 0.1$. Term (iii) is the viscous stress associated with the spatial variation in
231 $<\overline{u}>$. The final term, D_x, is the spatially-averaged drag associated with the canopy elements, which
232 is often represented by a quadratic drag law (*e.g*. Kaimal & Finnegan 1994, p. 95).

233

234
$$D_x = \frac{1}{2}\frac{C_D a}{n}\langle\overline{u}\rangle\left|\langle\overline{u}\rangle\right| \qquad (9)$$

235

236 The canopy-drag length-scale, L_c, is defined from the quadratic drag law. Based on dimensional

237 reasoning $D_x = \langle \bar{u} \rangle^2 / L_c$ (Belcher et al. 2003). From (9)

238

239 $$L_c = \frac{2(1-\phi)}{C_D a}. \qquad (10)$$

240

241 This represents the length-scale over which the mean and turbulent flow components adjust to the

242 canopy drag. Since, most aquatic canopies have high porosity ($\phi < 0.1$), this scale is commonly

243 approximated by $2(C_D a)^{-1}$.

244

245 3.1 Stem-scale turbulence

246 Branches and stems with an orientation that is perpendicular to the flow can generate

247 turbulence. The stem diameter (or blade width) d defines the stem Reynolds' number, $Re_d = Ud/\nu$.

248 For $Re_d > \approx 100$, the canopy elements will generate vortices of scale d, which is called stem-scale

249 turbulence (*e.g.* Nepf 2012 and references therein). If the stem density is high, such that the mean

250 spacing between stems (ΔS) is less than d, the turbulence is generated at the scale ΔS (Tanino and

251 Nepf 2008). Even for very sparse canopies, the production of turbulence within stem wakes is

252 comparable to or greater than the production by bed shear (Nepf *et al.* 1997, Burke & Stolzenbach

253 1983, Lopez & Garcia 1998). Therefore, turbulence level *cannot* be predicted from the bed-friction

254 velocity, as it is for open-channel flow. Instead, it is a function of the canopy drag. Vortex

255 generation in stem wakes drains energy from the mean flow (expressed as mean canopy drag) and

256 feeds it into the turbulent kinetic energy. If this conversion is 100% efficient, then the rate at which

turbulent energy is produced is equal to the rate of work done by the flow against canopy drag (Raupach and Shaw 1982). If we further assume that the energy is extracted at the length-scale ℓ, the turbulent kinetic energy (k) in the canopy may be estimated from (Tanino and Nepf 2008),

$$\frac{\sqrt{\langle \bar{k} \rangle}}{\langle \bar{u} \rangle} \approx \left(C_D \frac{\ell}{d} \frac{2\phi}{(1-\phi)\pi} \right)^{1/3}. \qquad (11)$$

Here, ℓ is the smaller of d or ΔS. In fact, only the form drag is converted into turbulent kinetic energy. The viscous drag is dissipated directly to heat. For stiff canopies, or near the rigid base of most stems, the drag is mostly form drag, and (11) is a reasonable approximation. However, in the streamlined portion of flexible submerged plants the drag is predominantly viscous, and (11) would be an overestimate of stem-scale turbulence production (Nikora & Nikora 2007).

An interesting non-linear behavior emerges when we compare conditions of different stem density under the same driving force (*i.e.* the same potential and/or pressure gradient). The details of this comparison are given in Nepf (1999). Because the vegetation offers resistance to flow, the velocity within a meadow is always less than the velocity over a bare bed under the same external forcing, and the canopy velocity decreases monotonically with increasing stem density (or ϕ). However, changes in turbulent kinetic energy, $< \bar{k} >$, reflect competing effects as stem density (ϕ) increases, *i.e.* turbulence intensity, $< \bar{k} > / < \bar{u} >^2$, increases, but $< \bar{u} >^2$ decreases, which together produce a non-linear response. As stem density (or ϕ) increases from zero, $< \bar{k} >$ initially increases, but eventually decreases as ϕ increases further. This non-linear response was predicted numerically for flow through emergent vegetation (Burke and Stolzenbach, 1983) and within submerged roughness elements (Eckman, 1990). It was also observed in a flume study of *Zostera Marina*

(Gambi *et al*., 1990). The fact that at some stem densities the near bed turbulence level within a meadow can be higher than over adjacent bare bed has important implications for sediment transport. This is discussed further in the next section.

3.2 Sparse and Dense Meadows

We now consider a submerged meadow of height h in water of depth H (Figure 2). For a submerged meadow, there are two limits of flow behavior, depending on the relative importance of the bed shear and meadow drag. If meadow drag is small compared to bed drag, then the velocity follows a turbulent boundary layer profile, with the vegetation contributing to the bed roughness. This regime is called a sparse meadow or canopy (Figure 2a). In this regime, the turbulence near the bed will increase as stem density increases. Alternatively, in the dense canopy regime the meadow drag is large compared to the bed stress, and the discontinuity in drag at the top of the meadow generates a region of shear resembling a free-shear-layer and notably including an inflection point near the top of the meadow (Figure 2b, c). From scaling arguments, the transition between sparse and dense regimes occurs at $\lambda = ah = 0.1$ (Belcher et al 2003). From measured velocity profiles, a boundary-layer form with no inflection point is observed for $C_D ah < 0.04$, and a pronounced inflection point appears for $C_D ah > 0.1$ (Nepf et al 2007). Since $C_D \approx 1$ the measured and theoretical limits are consistent.

If the velocity profile contains an inflection point, it is unstable to the generation of Kelvin-Helmoltz (KH) vortices (*e.g*. Raupach et al 1996). These structures dominate the vertical transport at the canopy interface (*e.g*. Gao et al. 1989, Finnigan 2000, Ghisalberti & Nepf 2002). These vortices are called canopy-scale turbulence, to distinguish it from the much-larger boundary-layer turbulence, which may form above a deeply submerged or unconfined canopy, and the much smaller

stem-scale turbulence. Over a deeply submerged (or terrestrial) canopy ($H/h > 10$), the canopy-scale vortices are highly three-dimensional due to their interaction with the boundary-layer turbulence, which stretches the canopy-scale vortices, enhancing secondary instabilities (Fitzmaurice et al. 2004, Finningan et al 2009). However, with shallow submergence ($H/h <= 5$), which is common in aquatic systems, larger-scale boundary-layer turbulence is not present, and the canopy-scale vortices dominate the turbulence both within and above the meadow (Ghisalberti & Nepf 2005, 2009).

Within a distance of about $10h$ from the canopy's leading edge, the canopy-scale vortices reach a fixed scale and a fixed penetration into the canopy (δ_e in Figure 2, Ghisalberti 2000, Ghisalberti & Nepf 2000, 2004, 2009). The final vortex and shear-layer scale is reached when the shear-production that feeds energy into the canopy-scale vortices is balanced by the dissipation by canopy drag. This balance predicts the following scaling, which has been verified with observations (Nepf et al. 2007).

$$\delta_e = \frac{0.23 \pm 0.6}{C_D a} \qquad (12)$$

Recall that $C_D ah \geq 0.1$ is required to produce shear-layer vortices, so that (12) applies only to those canopies. In the range $C_D ah = 0.1$ to 0.23, the shear-layer vortices penetrate to the bed, $\delta_e = h$, creating a highly turbulent condition over the entire canopy height (Figure 2b). At higher values of $C_D ah$ the canopy-scale vortices do not penetrate to the bed, $\delta_e < h$ (Figure 2c). If the submergence ratio $H/h < 2$, δ_e is diminished from (12), as interaction with the water surface diminishes the strength and scale of the vortices (Nepf & Vivoni 2000, Okamoto & Nezu 2009).

The penetration length, δ_e, segregates the canopy into an upper layer of strong turbulence and rapid renewal and a lower layer of weak turbulence and slow renewal (Nepf & Vivoni 2000, Nepf et al 2007). Flushing of the upper canopy is enhanced by the canopy-scale vortices that penetrate this region. In contrast, turbulence in the lower canopy ($z < h-\delta_e$) is generated in stem wakes and has significantly smaller scale, set by the stem diameters and spacing. Canopies for which $\delta_e/h < 1$ (Figure 2c) shield the bed from strong turbulence and turbulent stress. Because turbulence near the bed plays a role in resuspension, these dense canopies are expected to reduce resuspension and erosion. Consistent with this, Moore (2004) observed that resuspension within a seagrass meadow was reduced, relative to bare-bed conditions, only when the above ground biomass per area was greater than 100 g/m^2 (dry mass). This biomass corresponds to $ah = 0.4$ (Luhar et al. 2008). In a similar study, Lawson et al (2012) measured sediment erosion in beds of different stem density. Using the blade length (8 cm) and width (3mm) provided in that paper, we convert the stem density into a roughness density ah. Between 80 and 300 stems m^{-2} ($ah = 0.02$ to 0.07) erosion increased with increasing stem density, consistent with sparse canopy behavior, *i.e.* stem-scale turbulence augmented the near-bed turbulence, and increased with increasing stem density. However, above 500 stems m^{-2} ($ah = 0.12$) bed erosion was essentially eliminated within the meadow (Lawson et al. 2012). Both the Moore and Lawson studies demonstrate a stem density threshold, above which the near bed turbulence becomes too weak to generate resuspension and erosion. The threshold is roughly consistent with the roughness density transition suggested by (12) and depicted in Figure 2.

The regimes depicted in Figure 2 give rise to a feedback between optimum meadow density and substrate type. Because dense canopies reduce near-bed turbulence, they promote sediment retention. In sandy regions, that tend to be nutrient poor, the preferential retention of fines and organic material, *i.e.* muddification, enhances the supply of nutrient to the canopy, so that dense

canopies provide a positive feedback to canopy health in sandy regions (*e.g*. van Katwijk et al 2010). In contrast, in regions with muddy substrate, which is more susceptible to anoxia, sparse meadows ($C_D ah \leq 0.1$) may be more successful, because the enhanced near-bed turbulence removes fines, leading to a sandier substrate that is less prone to anoxia.

Both the boundary layer profile of a sparse canopy regime and the mixing layer profile of the dense canopy regime have been observed in the field, in seagrass meadows (Lacy 2011) and in river meadows (Sukhodolov and Sukhodolova 2010). Although both profiles have been observed in the field, modeling efforts have focused on the dense canopy limit. Most methods divide the flow into a uniform layer within the vegetation and a logarithmic profile above the vegetation. Given the poor scale-separation between plant height and flow depth, it is unlikely that a genuine logarithmic layer exists in aquatic flows over vegetation. However, previous studies have shown that a logarithmic profile provides a reasonable description of the velocity above a meadow for $H/h > 1.5$ (*e.g*. Nepf and Vivoni 2000, Poggi et al. 2004a). The roughness and displacement heights, as well as the friction velocity of the logarithmic profile above a canopy have been parameterized using characteristics of the vegetation (*e.g*. Kaimal and Finnigan 1994, Luhar et al. 2008, and references therein). A number of studies have proposed models for the full velocity profile, *i.e*. both within and above the bed. These studies utilize three general approaches: (i) simple momentum balances that segregate the flow into a vegetated layer of depth h and an overflow of depth H-h (*e.g*. Stone 2002, Huthoff 2007, Cheng 2011); (ii) analytical descriptions using an eddy viscosity model, ν_t, to define the turbulent stress (*e.g*. Meijer 1998, Baptiste 2007, Poggi 2009); and (iii) numerical models with first- or second-order turbulence closures (*e.g*. Shimizu & Tsujimoto 1994, Lopez & Garcia 2001, Rowinski 2002, Neary 2003, Defina & Bixio 2005). Some of the models reflect the bending response of flexible vegetation, by solving iteratively for the meadow height and velocity profile

(Dikstra & Uittenbogaard 2010, Luhar and Nepf 2012).

4. Emergent canopies of finite width and length

The previous section described the flow near a submerged canopy that was fully developed and uniform in the horizontal plane. While the fully developed case is important, it is not representative of all field conditions. For meadows of finite width and length, the regions of flow transition at the boundaries must also be understood. A few recent studies have begun to describe the flow structure near the leading and trailing edges of a meadow; at the edges of long meadows; and within the gaps between meadows (*e.g.*, Sukhodolov and Sukhodolova, 2010, Neumeier, 2007; Folkard, 2011; Zong and Nepf, 2010; Siniscalchi et al 2012). In this section, we consider geometries that are finite in length and width. We begin with emergent canopies, *i.e.* the plant occupies the full water depth.

4.1 Long emergent canopies of finite width

In river channels, emergent vegetation often grows along the bank, creating long regions of vegetation of finite width b (Figure 3). This configuration is geometrically similar to a submerged meadow of height h (= b). Long patches of vegetation may also exist at the center of a channel, and to recognize the geometric similarity with bank vegetation, we define b as the half-width for in-channel vegetation (Figure 4). Let the stream-wise coordinate be x, with $x = 0$ at the leading edge. The lateral coordinate is y, with $y = 0$ at the side boundary for bank vegetation (Figure 3), or at the centerline for in-channel vegetation (Figure 4). The streamwise and lateral velocity are (u,v), respectively. Because the vegetation provides such high drag, relative to the bare bed, much of the flow approaching the patch from upstream is diverted away from the patch. The diversion begins upstream of the patch over a distance that is set by the scale b, and it extends a distance x_D into the

393 vegetation (Zong and Nepf, 2010). Rominger and Nepf (2011) show that x_D scales with the larger of
394 the two length-scales b or $L_c = 2(C_D a)^{-1}$. It is only after the diversion is complete ($x > x_D$), that the
395 shear layer with KH vortices develops along the lateral edge of the vegetation. As discussed above,
396 similar structures form at the top interface of submerged vegetation, and, as also noted for
397 submerged meadows, the KH vortices at the edge of emergent meadows dominate the mass and
398 momentum exchange between the vegetation and the adjacent open flow (White and Nepf 2007).
399 The initial growth and the final scale of the horizontal shear-layer vortices and their lateral
400 penetration into the patch, δ_L, are depicted in Figure 3. The shear layer vortices extend into the open
401 channel over the length-scale δ_o. White and Nepf (2007) show that $\delta_o \sim H/C_f$, where H is the flow
402 depth and C_f is the bed friction. There is no direct relation between δ_L and δ_o. As expected from the
403 discussion of vertical canopy-shear layers, $\delta_L \sim (C_D a)^{-1}$. However, the scale factor observed for
404 lateral shear-layers (denoted by subscript L) is twice that measured for vertical shear layers above
405 submerged meadows (δ_e, Figure 2, eq. 12). Based on White and Nepf (2007, 2008)
406
407 $$\delta_L = \frac{0.5 \pm 0.1}{C_D a} \qquad (13)$$
408
409 The difference between δ_L and δ_e may be due to the difference in flow geometry relative to
410 the model canopy. Specifically, in experiments with vertical circular cylinders (as in White and
411 Nepf 2007), the cylinder presents a different geometry to vortices rotating in the horizontal plane
412 than to vortices rotating in the vertical plane. Also note that a wider range of canopy morphology,
413 including field measurements with real vegetation, and a wider range of flow speeds were used to
414 determine the scale factor for δ_e (Nepf et al. 2007). The scale factor for δ_L is based only on one set

of flume experiments with rigid circular cylinders. Whether, or not, the difference in the scale factor is significant for field conditions has not yet been determined.

The adjustment of the flow field to a long-patch of vegetation depends on two length-scales: patch width, b, and canopy drag, $L_c \approx 2(C_D a)^{-1}$. Together they form a dimensionless parameter, $C_D ab$, called the flow blockage. Note its similarity with the roughness density (ah). A transition in flow behavior occurs at the value $C_D ab = 2$ (Rominger and Nepf 2011). According to (13), if $C_D ab > 2$ (high flow blockage), the patch width, b, is greater than the penetration distance, δ_L, and the patch is segregated into two regions: an outer region ($y > b - \delta_L$) within which the KH vortices contribute to turbulent momentum exchange, and an inner region ($y < b - \delta_L$) with negligible turbulent stress. Because turbulent stress does not penetrate to the core of a high flow blockage patch, the velocity within the patch (U_1, Figure 3) is set by a balance of potential gradient (bed and/or water surface slope) and vegetation drag. In contrast, for patches of low flow blockage ($C_D ab < 2$), U_1 is set by the balance of turbulent stress and vegetation drag. Detailed formulations for U_1 under high and low flow blockage conditions are given in Rominger and Nepf (2011).

In addition to producing turbulent momentum flux, the KH vortices also induce a pressure response. Specifically, the center of each vortex is a point of low pressure, which, for shallow flows, induces a wave response across the entire patch, and specifically beyond δ_L from the edge (White and Nepf 2007, 2008). The wave response within the vegetation has been shown to enhance the lateral (y) transport of suspended particles, above that predicted from stem-turbulence alone (Zong and Nepf 2011). For in-channel patches, shear-layers develop along both flow-parallel edges producing a train of coherent vortices along each edge (Figure 4a), and observations indicate that these vortices interact across the canopy width. The low-pressure core associated with each vortex produces a local depression in the water surface, such that the passage of individual vortices can be

438 recorded by a surface displacement gage. A time record of surface displacement measured on
439 opposite sides of a patch (A1 and A2 in Figure 4b) show that there is a half-cycle phase shift (π
440 radians) between the vortex streets that form on either side of the patch. Because the vortices are a
441 half-cycle out of phase, when the pressure (surface displacement) is at a minimum on side A1, it is at
442 a maximum at side A2. The resulting cross-canopy pressure gradient induces a transverse velocity
443 within the canopy (Figure 4b) that lags the lateral pressure gradient by π/2, *i.e.* a ¼ cycle. The
444 synchronization of the vortex streets occurs even when the vortex penetration is less than the patch
445 width, $\delta_L/b < 1$, or $C_D ab > 2$ (high flow blockage), and it significantly enhances the vortex strength
446 and the turbulent momentum exchange between the open channel and vegetation (Rominger and
447 Nepf 2011). More importantly, the vortex interaction introduces significant lateral transport at the
448 center of the patch. For example, the data shown in Figure 4b corresponds to a patch with upstream
449 flow U_o = 10 cms^{-1} and centerline velocity U_1 = 0.5 cms^{-1}. The lateral velocity at the centerline
450 (induced by the vortex pressure field) was nearly one order of magnitude larger, with maximum
451 lateral velocities of 3.5 cm s^{-1} (v_{rms} = 2.2 cm s^{-1}, Figure 4b). Using the period of the vortex passage
452 (T = 10 s), the lateral excursion of a fluid parcel during each vortex cycle is 10 cm (= $v_{rms}T/2$). This
453 lateral excursion is comparable to the half-width of the patch, b = 10 cm, indicating that fluid parcels
454 in the center of the patch can be drawn into the free stream and vice versa, during each vortex
455 passage. This cycle of flushing can significantly reduce the patch retention time, and may even
456 control it. This is especially true when the aspect ratio of the canopy is greater than one, which is
457 typical in channel vegetation, *e.g.* Sand-Jensen and Pedersen (2008) report typical length-to-width
458 aspect ratios of 2.5. The reduced retention time has implications for plant fecundity, structural
459 stability, and habitat viability, and the transport and fate of pollutants and contaminants.
460

461 4.2. Circular patches of vegetation

462 A circular patch with diameter D (Figure 5) is used as a model for a vegetated region with
463 length and width smaller than the channel width. We still consider patches that are emergent, so that
464 the flow field is roughly two-dimensional (x-y). Because the patch is porous, flow passes through it,
465 which alters the wake structure relative to a solid body (Castro 1970, Chen and Jirka 1995, Ball et al.
466 1996, Takemura and Tanaka 2007). In the wake of a solid body, there is a region of recirculation
467 directly behind the body, followed by a von Karman vortex street. The wake-scale mixing provided
468 by the von Karman vortices allows the velocity in the wake to quickly return (within a few
469 diameters) to a velocity comparable to the upstream (U_o). In contrast, the wake behind a porous
470 obstruction (patch of vegetation) is much longer than that behind of solid body, because the flow
471 entering the wake through the patch (called the bleed flow), delays the onset of the von-Karman
472 vortex street. The velocity at the centerline of the wake, U_1, remains nearly constant over the
473 distance from the patch to the onset of the von Karman street. This distance, L_1, is called the steady
474 wake (Figure 5). The steady wake is a region of reduced velocity and turbulence, relative to the
475 adjacent bare bed, so that it is a region where deposition is likely to be enhanced. The connection
476 between the steady wake and deposition is described further in section 6.

477 The delayed onset of the von Karman vortex street can be visualized using traces of dye
478 injected at the outermost edges of the patch. This is shown schematic in Figure 5. Because the
479 steady wake is fed only by water entering from upstream through the patch, there is no dye in this
480 region, *i.e*. the steady wake appears as a clear region directly behind the patch, in between the two
481 dye streaks. After distance L_1, the two dye streaks come together, and a single, patch-scale, von-
482 Karman vortex street is formed. Note that Figure 5 represents a single snapshot in time, capturing
483 one phase of the unsteady vortex cycle. As the vortex cores migrate downstream, the flow field at

484 any fixed point oscillates with frequency, f, which is set by the patch-scale D. The patch-scale
485 vortex street follows the same scaling as a solid body, with Strouhal number $St = fD/U_o \approx 0.2$ (Ball et
486 al 1996, Zong and Nepf 2012).

487 Near a porous patch there are two distinct regions of elevated turbulence. First, there is a
488 peak in turbulence within and directly behind the patch, associated with the stem-scale turbulence
489 generated in the wakes of individual stems. However, these small eddies die out quickly with
490 distance from the patch, so that the steady wake is a region of low turbulence. A second maximum
491 in *TKE* appears with the formation of the patch-scale vortices. The magnitude of turbulence in this
492 second peak increases with increasing flow blockage (Zong and Nepf 2012).

493 Both U_1 and L_1 can be predicted from the flow blockage, which is defined as $C_D aD$ for the
494 circular patch geometry (Chen et al. 2012). Recognizing that $D = 2b$, we expect that for a circular
495 patch there is a transition in flow behavior near $C_D aD = 4$. This transition is apparent in the
496 dependence of U_1 on $C_D aD$ (Figure 5). For low flow blockage (small $C_D aD$), U_1/U_o decreases
497 linearly with $C_D aD$. Using $C_D = 1$, a reasonable linear fit is,

498

499 $$\frac{U_1}{U_o} = 1 - [0.33 \pm 0.08] C_D aD \qquad (14)$$

500

501 For high flow blockage, U_1 is negligibly small ($U_1/U_\infty \approx 0.03$), but not zero. However, at some point
502 around $C_D aD = 10$, U_1 becomes zero, and the flow field around the porous patch is identical to that
503 around a solid obstruction (Zong and Nepf, 2012; Nicolle and Eames, 2011). This transition is also
504 seen in the length-scale, L_1, discussed below.

505 The flow in the steady wake (U_1) separates two regions of faster velocity (U_2), creating a
506 shear layer on either side of the steady wake. These layers grow linearly with distance from the

patch (depicted by thin lines in Figure 5), eventually meeting at the wake centerline. When the shear layers meet, they interact to form the von Kármán vortex street. Thus, L_1 may be predicted from the growth of the linear shear layers. Based on this Zong and Nepf (2012) derived,

$$\frac{L_1}{D} = \frac{1}{4S_1}\frac{(1+U_1/U_2)}{(1-U_1/U_2)} \approx \frac{1}{4S_1}\frac{(1+U_1/U_o)}{(1-U_1/U_o)} \quad (15)$$

S_1 is a constant (0.10±.02) across a wide range of D and ϕ (Zong and Nepf, 2012). If the channel width is much greater than the patch diameter, we may assume that $U_2 \approx U_O$, resulting in the right-most equation in (15). Predictions for L_1/D based on (14) and (15) do a good job representing the observed variation in L_1 with C_DaD (Figure 4b). Note that even as the velocity behind the patch approaches zero, the delay in the vortex street persists, with $L_1/D = 2.5$. However, when C_DaD becomes high enough that there is no bleed flow ($U_1 = 0$), the wake resembles that observed for a solid body, with a recirculation zone and vortex street forming directly behind the patch, so that $L_1 \approx 0$. The data shown in Figure 6 suggests that this occurs for $C_DaD > 10$. Nicolle and Eames (2011) also observed this transition in numerical simulations. Based on Figure 10 of their paper, the wake resembles that of a solid-body for $\phi \geq 0.22$, with $D/d = 21$, $C_D = 1.6$ (based on information given in *Nicolle and Eames*, 2011), so that their transition corresponds to $C_DaD = (4/\pi)\,C_D\,\phi\,(D/d) = 9$. This is consistent with the transition inferred from the data set shown here (Figure 6).

The wake transition described above has implications for the characterization of drag contributed by finite patches. As noted by Folkard (2010), drag is produced at two distinct scales; the leaf and stem scale, and the patch scale. For low flow blockage patches, there is sufficient flow through the patch that the stem and leaf scale drag dominates the flow resistance, *i.e.* the flow resistance can be represented by the integral of C_Dau^2 over the patch interior, with u the velocity

within the patch. However, for high flow blockage patches, there is negligible flow through the patch, and the integral of $C_D a u^2$ over the patch interior is irrelevant. As revealed by the wake structure, the flow response to a high flow-blockage patch is essentially identical to the flow response to a solid obstruction of the same patch frontal area, A_p. Thus, the flow resistance provided by the patch should be represented by the patch-scale geometry, *i.e.* $C_D A_p U^2$, with U the channel velocity. This idea is supported by measurements of flow resistance produced by sparsely distributed bushes (Righetti and Armanini 2002, Righetti 2008). A bush consists of a distribution of stems and leaves, and so is a form of vegetation patch. The flow resistance generated by the bushes, D_B, was shown to fit the model, $D_B = \rho C_D A_p U^2$, and notably C_D was O(1), simlar to a solid body. Thus, although porous, the bush generated drag that was comparable to that of a solid object of the same size (A_P). It is worth noting that C_D decreased somewhat (from 1.2 to 0.8) as the channel velocity increased. This shift is most likely due to the reconfiguration of stems and leaves that reduced A_P. Since this reconfiguration was not accounted for in the analysis, it shows up as an apparent decrease in C_D. More studies are needed to explore the transition between flow resistance dominated by stem (leaf) -scale drag to flow resistance dominated by patch-scale drag. In the next section, we consider flow resistance at the channel reach scale, and again find that patch-scale geometry is more important than leaf-scale geometry.

5. Reach scale hydraulic resistance –

Field studies by Green (2005b) and Nikora et al. (2008) suggest that at the scale of the channel reach, flow resistance due to vegetation is determined primarily by the blockage factor, B_X, which is the fraction of the channel cross-section blocked by vegetation. For a patch of height h and width w in a channel of width W, and depth H; $B_x = wh/WH$. The studies show strong correlations

553 between B_x and Manning roughness coefficient, n_M, noting that the relationship between n_M and B_x is
554 nonlinear. These observations are in agreement with Ree (1949) and Wu et al. (1999), who showed
555 that roughness in channels lined with vegetation is influenced primarily by the submergence ratio,
556 H/h. For vegetation that fills the channel width, $B_x = h/H$. Luhar et al. (2008) presented a
557 momentum balance model that explains the nonlinear relationship between n_M and B_X. However, a
558 few studies suggest that in addition to the total flow blockage (B_x), the vegetation distribution may
559 also influence the resistance, and specifically that greater resistance is produced by distributions with
560 a greater interfacial area between vegetated and unvegetated regions (*e.g*. Vereecken et al. 2006, Bal
561 et al. 2011). Luhar and Nepf (2012) quantified the impact of interfacial area by considering
562 channels with the same blockage (B_x), but a different number (N) of patches. As the number of
563 patches (N) increased, the length of interfacial area also increased, which led to an increase in
564 channel resistance. However, observations made in natural rivers (Green 2006, Naden et al. 2006,
565 Sukhodolov and Sukhodolova 2010) suggest that a realistic upper bound for the number of patches
566 in a channel cross-section is $N = 5$, for which resistance increased by at most 20%, relative to $N = 1$.
567 Based on this, Luhar and Nepf (2012) suggest that $N = 1$ is a reasonable simplifying assumption
568 (with up to 20% uncertainty). Then, from momentum balance the following equations for Manning
569 roughness can be derived.
570

571 For $B_x = 1$: $$n_M\left(\frac{g^{1/2}}{KH^{1/6}}\right) = \left(\frac{C_D a H}{2}\right)^{1/2} \quad (17)$$

572 For $B_x < 1$: $$n_M\left(\frac{g^{1/2}}{KH^{1/6}}\right) = \left(\frac{C}{2}\right)^{\frac{1}{2}}\left(1 - B_x\right)^{-\frac{3}{2}} \quad (18)$$

573

574 The constant $K = 1\ m^{1/3}\ s^{-1}$ is required to make the equations dimensionally correct. Note that (17) is

valid when $B_x = 1$, which indicates that vegetation covers the entire cross-section, width and depth. The coefficient C parameterizes the shear stress at the interface between vegetated and unvegetated regions, and $C = 0.05$ to 0.13, based on fits to field data (Luhar and Nepf 2012). While (18) seems attractively simple, remember that for flexible vegetation B_x (= wh/WH) will be a function of flow speed, because the meadow height, h, decreases as flow speed increases. To use (18) for field predictions, one needs the physical characteristics of the vegetation, specifically the buoyancy and rigidity, to estimate the meadow height, h, from equation (6).

It is instructive to consider the case of submerged vegetation that fills the channel width, such that the resistance is a function only of the submergence depth (H/h). This case has been considered in many classic papers of channel resistance, such as Ree (1949) and Wu et al (1999). For this case, the Mannings coefficient may be represented as (Luhar and Nepf 2012),

For $H/h > 1$:

$$n_M\left(\frac{g^{1/2}}{KH^{1/6}}\right) = \left[\left(\frac{2}{C}\right)^{\frac{1}{2}}\left(1-\frac{h}{H}\right)^{\frac{3}{2}} + \left(\frac{2}{C_D a h}\right)^{\frac{1}{2}}\frac{h}{H}\right]^{-1} \qquad (19)$$

If $C_D ah > C$, a common field condition, the second term drops out and (19) reverts to (18), because for vegetation covering the full channel width, $B_x = h/H$.

Several researchers have noted a non-linear relationship between n_M and a form of channel Reynolds number, VR, with V the channel average velocity and R the hydraulic radius (*e.g.* Ree 1949, Gourlay 1970). Folkard (2011) provides a useful discussion of this relationship, noting that the peak in hydraulic resistance occurs at the transition from emergent to submerged conditions. Because most channel vegetation is flexible, an increase in velocity is associated with a decrease in vegetation height, *i.e.* $h \sim 1/V$. In addition, for wide channels, $R = H$, so that $H/h \sim VR$. This

suggests that the observed trends of n_M with VR can be mostly explained by the trends of n_M with H/h, as expressed through (17), for emergent conditions, and (19), for submerged conditions. As an example, n_M was calculated from (17) and (19) using $C_D ah = 10$ and $C = 0.1$ (Figure 7). If the plants are emergent ($H/h < 1$), vegetation drag increases with increasing depth ratio (H/h), because the total vegetation area per bed area (aH) increases as H/h increases (17). However, if the plants are submerged ($H/h > 1$), the hydraulic resistance decreases as H/h increases. This is made more obvious by noting that as H/h increases above 1, the second term in (19) quickly becomes negligible, reducing to $n_M = \left(C/2\right)^{\frac{1}{2}}\left(1 - H/h\right)^{-\frac{3}{2}}$. The curve shown in Figure 7 is visually similar to the many empirical curves presented for n_M versus VR (*e.g.* Ree 1949, Wu et al 1999, Folkard 2010). Finally, for flexible vegetation, we can capture the effect of reconfiguration on (19) by using the relationships discussed in section 2.2. In the terms related to flow blockage (h/H), h can be predicted from (6). In the term related to vegetation drag, $C_D ah$ is replaced by $C_D a\, l_e$, with l_e determined from (5). The solution is iterated through predictions of n_M, U, and h and l_e until convergence.

6. Sediment transport and channel evolution

By baffling the flow and reducing bed-stress, vegetation creates regions of sediment retention (*e.g.* Abt et al. 1994, Lopez and Garcia 1998, Cotton et al. 2006, Gurnell et al. 2006). In some channels vegetation retains 80% of the sediment in transit downstream (Sand-Jensen 1998). Tal and Paola (2007) showed that single-thread channels are stabilized by vegetation. Similarly, Braudrick et al. (2009) showed that vegetation helps to maintain a meandering channel form. It is now clearly recognized that vegetation can enhance channel stability (Afzalimehr and Dey 2009; Li and Millar 2010; Wang et al. 2009, Pollen-Bankhead and Simon 2010; Wynn and Mostaghimi 2006a) and reduce sediment loading from bank erosion (Lawler 2008).

620 Because of the positive impacts vegetation provides for water quality, habitat and channel
621 stability, researchers now advocate replanting and maintenance of vegetation in rivers (*e.g*., Mars et
622 al. 1999, Pollen and Simon 2005). However, to design restoration schemes that will be sustainable,
623 we need a better understanding of how the distribution and density of vegetation determines channel
624 stability (Naden et al. 2006). Similarly, numerous publications (*e.g*. NRC 2002) and government
625 policies (CBEC 2003) advocate for fluvial vegetation as traps for sediments and other pollutants, but
626 few studies have measured actual storage rates (Noe and Hupp 2009). These gaps in understanding
627 must be addressed through collaborations between fluvial hydraulics and geomorphology.
628 Most previous studies observe enhanced deposition in regions of vegetation, with greater
629 accretion observed in regions of higher stem density (*e.g*., Bos et al. 2007). The capture of particles
630 within regions of vegetation enhances the retention of organic matter, nutrients and heavy metals
631 within a channel reach (*e.g*. Schultz et al., 2003; Brookshire and Dwire, 2003; Windham et al.,
632 2003). However, some recent studies have also noted regions of erosion that develop at the edges of
633 vegetation, because, as flow is diverted away from the vegetation, it must accelerate along the edges
634 (Bouma et al. 2007, Rominger et al. 2010). The redistribution of flow also produces spatial patterns
635 in sediment texture, with fine grain sediment and organic matter accumulating within patches, where
636 velocity is reduced, and coarse grain sediment left between the patches, where velocity is enhanced
637 (Sand-Jensen and Madsen 1992). The degree of sediment redistribution is a function of the stem
638 density within the vegetated area (Sharpe and James 2006, Mudd et al. 2010). The opposite trend
639 has also been observed, *i.e*. the removal of fines from within a patch. Specifically, van Katwjk et al
640 (2010) observed that sparse patches of vegetation were associated with sandification, a decrease in
641 fine particles and organic matter, which is most likely attributed to higher levels of turbulence within
642 the sparse patch, relative to adjacent bare regions. If the stem density is sufficiently low, so that the

643 velocity within the patch remains high, turbulence generation within the wakes of individual stems
644 increases the turbulence levels within the patch (Nepf 1999), which inhibits deposition (Zong and
645 Nepf 2012). In addition, a horseshoe vortex forms at the base of each stem (Liu et al. 2008; Nepf
646 and Vivoni 2000), creating a local region of elevated turbulence and bed-shear stress, and producing
647 scour holes around individual plants (Rominger et al. 2010, Figure 8), although the impact of this on
648 spatially averaged sediment transport has not yet been described.

649 Elevated turbulence levels have also been observed within the leading edge of a patch,
650 resulting in net deposition that is lower within the leading edge than in the adjacent bare bed, despite
651 the fact that the mean flow is reduced (Zong and Nepf 2011, 2012, Cotton et al. 2006). At the same
652 time, deposition of fine sediment has been observed in the wake behind a patch (Chen et al, 2012),
653 which, together with the diminished deposition near the leading edge, may explain why patches
654 grow in length predominantly in the downsteam direction (Sand-Jensen and Madsen 1992). Further,
655 observations given in Chen et al (2012) suggest that the deposition of fine material is limited to the
656 steady wake (L_l in Figure 5) where both the mean and turbulent velocities are depressed. The
657 formation of the von Karman vortex street at the end of the steady wake significantly elevates the
658 turbulence level, inhibiting deposition. By extension, we conjecture that the onset of the von
659 Karman vortex street may set the maximum length of enhanced deposition behind a patch, and
660 potentially the maximum streamwise extension of a patch. The lateral growth of a patch may also be
661 influenced by a hydrodynamic control. Specifically, the diversion of flow around a vegetated region
662 produces locally enhanced flow at its edges that promotes erosion and inhibits its lateral expansion
663 (Fonseca et al., 1983; Temmerman et al., 2007; Bennett et al. 2008, Bouma et al., 2009; Rominger
664 and Nepf, 2011). These examples of the interplay between flow and patch growth demonstrate
665 feedbacks between vegetation, flow and geomorphology. There is much to be learned about these

666 feedbacks. Yet, this understanding is vital in the planning of successful restoration projects.

667 Setting aside the complexity of heterogeneous vegetation discussed above, even for
668 homogeneous regions of uniform vegetation we lack a good description of sediment transport. This
669 is currently hampered by two problems. First, while it is tempting to apply sediment transport
670 models developed for open channel flow to predict sediment transport in regions of vegetation, it is
671 not clear that this is a valid approach. Open channel flow models relate sediment transport to the
672 mean bed stress (*e.g.* Julien 2010). However, new studies point to the important role of turbulence
673 in initiating sediment motion (*e.g.* Nino and Garcia 1996, Papanicolaou et al. 2002, Vollmer and
674 Kleinhans 2007, Celik et al 2010). In an open channel, the turbulence is directly linked to the mean
675 bed stress, so that traditional sediment transport models, based on the bed shear stress, may
676 empirically incorporate the role of turbulence into their parameterization. However, in vegetated
677 regions, the turbulence level is set by the vegetative drag and has little or no link to the bed shear
678 stress (*e.g.* Nepf 1999). If turbulence has any role to play in sediment transport, then we cannot
679 expect that relationships developed for open channel flow will hold in regions with vegetation. The
680 second problem we face in trying to characterize sediment transport within vegetation is that we lack
681 a reliable method for predicting the mean bed shear stress within a region of vegetation. Further,
682 there is significant spatial variability in bed stress at the scale of individual stems, *e.g.* similar to that
683 observed around piers (Escauriaza and Sotirpoulos 2011). The spatial pattern of bed stress imposed
684 by the stems is revealed, in part, by the scour holes observed around individual stems (*e.g.* Bouma et
685 al. 2007). Indeed, in sand-bed rivers, the addition of vegetation can lead to a transition in bed forms,
686 from migrating dunes to fixed patterns of scour associated with individual plants or stems (e.g.
687 Rominger et al 2010, Figure 8). To the extent that migrating dunes contribute to sediment transport,
688 the elimination of this migration will certainly impact bed-load transport.

689

690 6.1 Bed shear stress within a uniform canopy of vegetation

691 If we compare channels with and without vegetation, but with the same potential forcing, the
692 shear stress acting on the bed, represented by the friction velocity $u_* = \sqrt{\tau_{bed}/\rho}$, is reduced in the
693 presence of vegetation. This is reflected in the ratio $u_*/\sqrt{gHS}$, with S describing the slope of the
694 bed and/or water surface. This ratio is 1 for open channel flow and less than 1 in a vegetated
695 channel. Using a k-ε model to represent flow through rigid submerged vegetation (H/h = 3), Lopez
696 and Garcia (1998) show that this ratio drops off steadily with increasing aH (and thus ah),
697 approaching $u_*/\sqrt{gHS}$ = 0.1 at aH = 3 (ah = 1). That is, the bed stress with vegetation is reduced to
698 just 10% of the bare bed value. This dramatic reduction in bed stress is the main reason for reduced
699 sediment transport in vegetated flow zones (Lopez and Garcia, 1998).

700 While it is not yet clear that sediment transport within vegetation can be predicted from bed
701 shear stress alone, it is reasonable to expect bed stress will play a contributing role. Therefore, it is
702 useful to consider methods for estimating this parameter in the field. Several methods for estimating
703 bed shear stress have been developed and tested for open channel flow. However, most of these
704 methods do not apply in the presence of vegetation, because the presence of the vegetation
705 profoundly alters the vertical profiles of turbulence and mean flow. In the following paragraphs, we
706 discuss five methods.

707 First, the bed stress is defined by the spatial average of the viscous stress at the bed,

708

709 $$\tau_{bed} = \rho u_*^2 = \left\langle \nu \left. \frac{\partial \overline{u}}{\partial z} \right|_{z=0} \right\rangle. \qquad (20)$$

710

711 However, to properly define $\partial\overline{u}/\partial z$ at the bed, the measurement of velocity must be within the
712 laminar sub layer. While this is possible in a laboratory setting, it is rarely possible (or practical) to
713 make this fine-scale measurement in the field.

714 Second, for open channel flow, the bed stress can be easily estimated from the maximum,
715 near-bed Reynolds stress, or by extrapolating the linear profile of Reynolds stress to the bed (*e.g.*
716 Nezu and Rodi, 1986). We might adapt this method to vegetated regions by imposing the spatial
717 averaging described above, $\tau_{bed} = \rho u_*^2 = \left\langle \overline{u'w'} \right\rangle_{\max}$. However, in many vegetated flows, the near-
718 bed turbulent stress is zero, or close to it (*e.g.* Lopez and Garcia 1998, Nepf and Vivoni 2000,
719 Siniscalchi et al. 2012), making this estimator difficult to resolve in the field.

720 Third, turbulence in an open channel is produced by the boundary shear, so that there is a
721 direct link between the bed shear stress and near-bed *TKE* ($= 0.5(\overline{u'^2} + \overline{v'^2} + \overline{w'^2})$). Observations
722 over bare bed suggest $\tau_{bed}/\rho = u_*^2 \approx 0.2\ TKE$ (Stapleton and Huntley 1995, Rowinski et al. 2005).
723 Although this method has been used to estimate bed stress within regions of vegetation (*e.g.*
724 Widdows et al. 2008), it is questionable whether the method is valid over vegetated surfaces. Within
725 vegetation, turbulence is produced predominantly in the wakes of individual stems and branches, and
726 within the shear layer at the top of submerged meadows (section 3). There is no physical reason that
727 τ_{bed} and *TKE* should be correlated, because the contribution of bed shear to turbulence generation
728 within canopy is small to negligible (*e.g.* Nepf and Vivoni 2000). The lack of correlation between
729 *TKE* and u_* is clearly demonstrated by recent measurements (F. Kerger, unpub. data). Using an
730 LDV positioned to achieve high vertical resolution near the bed, the bed stress in a channel with
731 rigid emergent dowels was estimated using (20). The ratio TKE/u_*^2 is plotted in Figure 9a. If an
732 extension from open channel conditions were valid, we expect $TKE/u_*^2 \approx 5$. However, within the
733 emergent arrays, TKE varies between 3 and 67, showing no clear trend with roughness density, *ah*.

734 This suggests that the estimator $u_*^2 = 0.2\ TKE$ is not valid within regions of vegetation.

735 Fourth, when vegetation is present, the total flow resistance can be partitioned between the
736 bed stress and the vegetation drag (*e.g*. Raupach 1992). Integrating the momentum equation (8) over
737 the flow depth, we can infer the bed stress by subtracting the vegetation drag from the total potential
738 forcing, ρgSH. For steady, uniform flow conditions,

739

740
$$\underbrace{\tau_{bed} = \rho u_*^2}_{\text{bed stress}} = \rho gSH + \underbrace{\int_{z=0}^{h} \frac{1}{2}\frac{\rho}{n} C_D a \langle \overline{u} \rangle \left| \langle \overline{u} \rangle \right| dz}_{\text{vegetation drag}} \qquad (21)$$

741

742 This method has been used by several authors (*e.g*. Nezu & Onitsuka 2001; Jordanova & James
743 2003, Larsen et al 2009, Schoneboom et al. 2010). The problem with this method is that the bed
744 stress is generally much smaller than either term on the right-hand side, making this estimator prone
745 to large errors. In addition, the method relies on accurate estimates of frontal area (a) and drag
746 coefficient C_D. These values are not known for many plant species.

747 A possible new estimator for bed stress within vegetation is based on the following
748 observations. If vegetation density is high enough ($ah > 0.1$), the velocity near the bed is vertically
749 uniform and is set by the vegetation drag (*e.g*. Lightbody and Nepf 2006, Liu et al 2008).
750 Specifically, the velocity is set by a balance of vegetation drag and potential forcing, yielding
751 $U_v = \sqrt{2gS/C_D a}$ (*e.g*. Nepf 2012). In some cases a velocity overshoot is observed near the bed,
752 associated with the junction vortex at the stem base (Liu et al. 2008). For the purpose of this simple
753 analysis, we neglect this overshoot. Because the stem turbulence has scale d, we may reasonable
754 assume that this turbulence is damped by viscous stress near the bed within a region $z < d$. This
755 implies that the velocity deviates from its uniform value at a distance from the bed that scales with d.

If the flow conditions within this region ($z < d$) are laminar, then we can estimate (20) using the scale $\partial u/\partial z|_{z=0} \sim U_v/d$. Then, (20) reduces to

$$u_*^2 \sim \frac{\nu U_v}{d} = \frac{\nu}{d}\sqrt{\frac{2gS}{C_D a}} \qquad (22)$$

The scale relation given in (22) was verified with measurements collected in uniform arrays of rigid, emergent cylinders. For simplicity, U_v is approximated by the depth-averaged velocity, U. In both studies (Zavistoski 1992, F. Kerger, unpublished data) the friction velocity was estimate from multiple vertical profiles using (20). For arrays of sufficient density ($ah > 0.1$), a consistent scale factor is suggested by the observations, $u_*^2 = [2.0 \pm 0.2]\nu U_v/d$. However, note that the data shown are limited to conditions with $Re_d < 1000$ and $Re_H < 15{,}000$, which covers only a small fraction of field conditions. Also, Ishikawa et al. (2003) directly measured the stress on a mobile bed within a region of circular cylinders, and they observed that the skin friction increased with increasing cylinder density, probably because the viscous region near the bed is thinned as the stem-generated turbulence becomes more vigorous. This implies that the scale factor in (22) may be a function of a. Clearly, more work is needed to understand the applicable limits of (22).

We conclude from the above review that there is much work needed to understand sediment transport within regions of vegetation. We lack a reliable method for estimating bed stress, and frankly, we are not even sure that the mean bed stress is the sole relevant parameter (*e.g.* Vollmer and Kleinhans 2007). We must also consider the role of turbulence (*e.g.* Nino and Garcia 1996, Celik et al 2010), and relevant to this, the turbulent structure in regions of vegetation is quite different from that over bare bed (*e.g.* Nepf 1999, 2000, Poggi et al. 2004a). Finally, the bed stress varies at the stem-scale, and this variability may play a role in setting the rates of sediment transport.

779

780 7. Conclusion and Future Directions:

781 This paper has covered a lot of ground, and still it has not touched on many important areas,
782 including: the interaction of waves with submerged and emergent grasses (*e.g*. Kobayashi et al 1993,
783 Mendez and Losada 2004, Lowe et al. 2005, Bradley and Houser 2009); the impact of vegetation on
784 mass transport at the meadow and reach scales (*e.g*. Harvey et al. 2003, Serra et al. 2004, Ghisalberti
785 and Nepf 2005, Sukhodolova et al. 2006, Murphy et al. 2007, Tanino and Nepf 2008, Huang et al
786 2008); and the dispersion and capture of pollen and seeds (*e.g*. Ackerman 1997, 2000; Chambert and
787 James 2009, Defina and Peruzzo 2010). Indeed, the volume of research in vegetation
788 hydrodynamics has exploded in recent years, as we realize the many environmental functions are
789 influenced by vegetation. To end, I will note three areas in which vegetation hydrodynamics can
790 play an important role; in resource management, environmental restoration, and carbon cycling.

791 *Restoration*: River and stream restoration seeks to return ecological function and biodiversity
792 to channels by stabilizing stream banks, improving water quality, and restoring in-stream habitat (US
793 EPA 2000). In the US alone, over $1 billion US dollars per year are spent on river restoration
794 projects (Bernhardt et al., 2005). Studies of previous restoration efforts point to the need for
795 collaboration between disciplines to design sustainable projects (Wohl et al. 2005, Palmer and
796 Bernhardt 2006), and vegetation is a central feature in many stream restoration and bank
797 stabilization efforts. For example, Bennett et al 2002 showed that the introduction of emergent
798 vegetation at fixed intervals, set at the estimated equilibrium meander interval, could provoke the
799 evolution of a straight channel toward a natural state of meandering. Similarly, Larsen and Harvey
800 (2010) explain how vegetation and sediment transport feedbacks drive landscape evolution in the
801 Everglades. Future research should continue to explore the feedbacks between vegetation spatial

802 distribution, flow, and landscape evolution, which is a critical component in the design of
803 conservation and restoration strategies for many aquatic systems.
804 *Hydraulics Resistance and Flood Management*: Vegetation was historically considered only
805 as a source of flow resistance and was frequently removed to reduce flooding. However, vegetation
806 provides ecological services that make it an integral part of river systems that must be maintained to
807 some extent. The trade-off between flood and ecological management underlines the need for a
808 reliable method to predict channel resistance in the presence of vegetation. The problem is
809 particularly pressing given that over half of the world's major river networks are regulated to manage
810 water resources and reduce flooding (Nilsson et al. 2005), and the frequency and magnitude of
811 storms is projected to increase due to climate change (Oki and Kanae 2006). For many years,
812 researchers have focused on characterizing flow resistance in channels with uniform distributions of
813 vegetation, emphasizing the drag contributed at the stem and leaf scale (*e.g.* Kouwen and Unny
814 1973, Kouwen 1990). However, this approach cannot work at the reach-scale, because at the reach
815 scale vegetation is rarely distributed uniformly, and the scale and spatial distribution of patches has
816 been shown to play an important role in the setting reach-scale flow resistance (*e.g.* section 5, and
817 discussion in Folkard 2010, Green 2005, 2006). It is the reach-scale resistance that is most relevant
818 for flood and watershed management. To properly address reach-scale flow resistance, we should
819 focus efforts in two key areas. First, we need to develop and validate methods to rapidly
820 characterize the spatial heterogeneity of vegetation at the reach scale (also noted by Folkard 2010).
821 Some promising methods are emerging within the fields of airborne remote sensing (*e.g.* Mertes,
822 2002); LIDAR imaging (*e.g.* Heritage and Milan, 2009); and other high-resolution optical methods
823 (Feurer *et al.* 2008a, b). Second, we need to understand what scale of morphologic detail is relevant
824 in the characterization of flow resistance. Recent studies point to spatial distribution at the patch-

825 scale, characterized by the blockage factor, as the key geometric element in characterizing drag at
826 the reach scale (section 5). But, we do not know the scale at which patch distribution must be
827 resolved. In other words, how sensitive is the prediction of reach-scale flow and resistance to the
828 resolution at which vegetation distribution is described? Or, more specifically, when are gaps
829 between patches sufficiently wide to producing channeling flow? What scale of channel must be
830 resolved to properly model the circulation within a marsh (e.g. Lightbody et al. 2008). These
831 questions could be addressed through a sequence of numerical experiments that examine the impact
832 of vegetation spatial scale on mean flow. Finally, because reconfiguration impacts the meadow
833 height, and thus the blockage factor, we must understand what level of morphological detail is
834 needed to properly predict reconfiguration, which in turn will require more detailed measurements of
835 plant material density and rigidity.

836 *Blue Carbon*: Salt marshes, mangrove forests, and seagrass meadows cover less than 0.5% of
837 the seabed, but account for 50 to 70% of the carbon storage in ocean sediments (Nellemann et al.
838 2009). How will the size of these habitats, and their potential for carbon storage, change with sea
839 level rise, with changes in coastal land use, changes in dam function (and its impact on sediment
840 supply)? Can we intentional build more marsh, mangrove, and seagrass habitat? The answer to
841 these questions will require knowledge of vegetation hydrodynamics. For example, the potential
842 carbon capture within a seagrass meadow depends on the photosynthetic rate, which in turn depends
843 on blade scale hydrodynamics (which sets nutrient flux) and blade/meadow scale reconfiguration
844 (which sets the posture of the plant, and thus influences light availability). The potential to build
845 new marsh will depend on our understanding the feedback between vegetation, flow and sediment
846 dynamics discussed in section 6.
847

848 To conclude, the proper management of many aquatic systems depends on understanding the impact
849 of vegetation on flow at different scales (blade, meadow, channel reach), which in turn impacts the
850 processes that establish and maintain important ecosystems (streams, seagrasses, marshes,
851 mangroves). Through collaborations in ecology, biology, geomorphology, and geochemistry, the
852 field of environmental hydraulics will answer important questions in environmental management.
853

854 **Acknowledgements-**

855 Some of this material is based upon work supported by the National Science Foundation under Grant
856 No. EAR0309188, EAR 0125056, EAR 0738352 and OCE 0751358. Any opinions, conclusions or
857 recommendations expressed in this material are those of the author(s) and do not necessarily reflect
858 the views of the National Science Foundation.
859

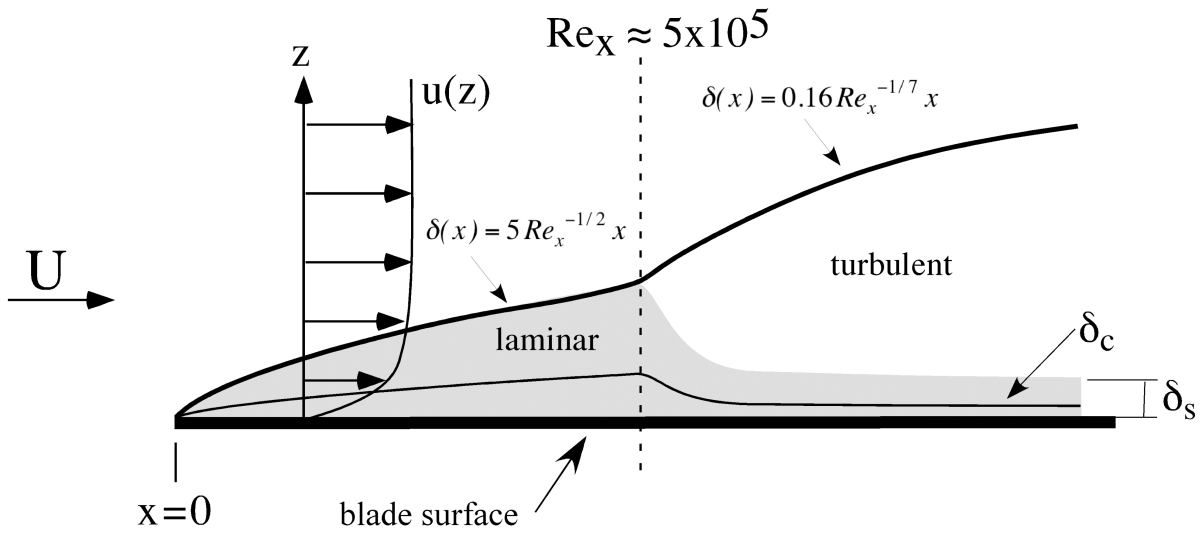

859

860

861 **Figure 1.** Evolution of a boundary layer on a flat plate. Vertical coordinate is exaggerated. The
862 momentum boundary layer, δ, grows with distance from the leading edge ($x = 0$). Initially the
863 boundary layer is laminar (shaded gray). At the distance, x, corresponding to $Re_x = xU/\nu \approx 5 \times 10^5$
864 the boundary layer becomes turbulent, except for a thin layer near the surface that remains laminar,
865 called the viscous (or laminar) sub-layer, δ_s. In water the diffusive sub-layer, δ_c, is much smaller
866 than the viscous sub-layer, with $\delta_c = \delta_s \, Sc^{-1/3}$. Figure from Nepf (2012a).

867

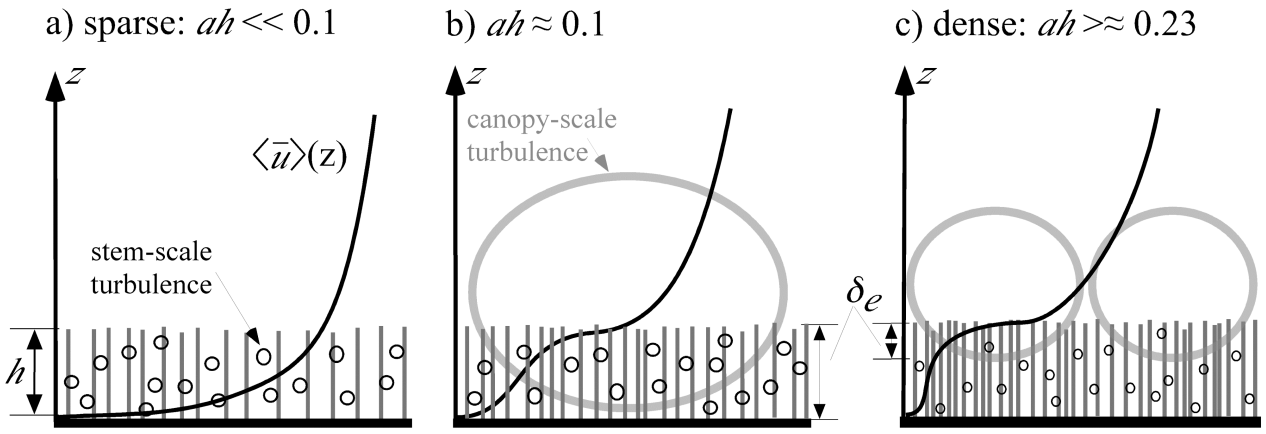

867

868 **Figure 2** Changes in the mean velocity profile through a submerged meadow with increasing
869 roughness density (ah). The meadow height is h. a) For $ah < 0.1$ (sparse regime), the velocity
870 follows a rough boundary layer profile. b) For $ah \geq 0.1$, a region of strong shear at the top of the
871 canopy generates canopy-scale turbulence. The canopy-scale turbulence penetrate a distance $\delta_e =$
872 $[0.23 \pm 0.06](C_D a)^{-1}$ into the canopy. c) For $ah > 0.23$ (dense regime), $\delta_e < h$, and the bed is shielded
873 from canopy-scale turbulence. Stem-scale turbulence is generated throughout the meadow. Adapted
874 from Nepf (2012b).

875

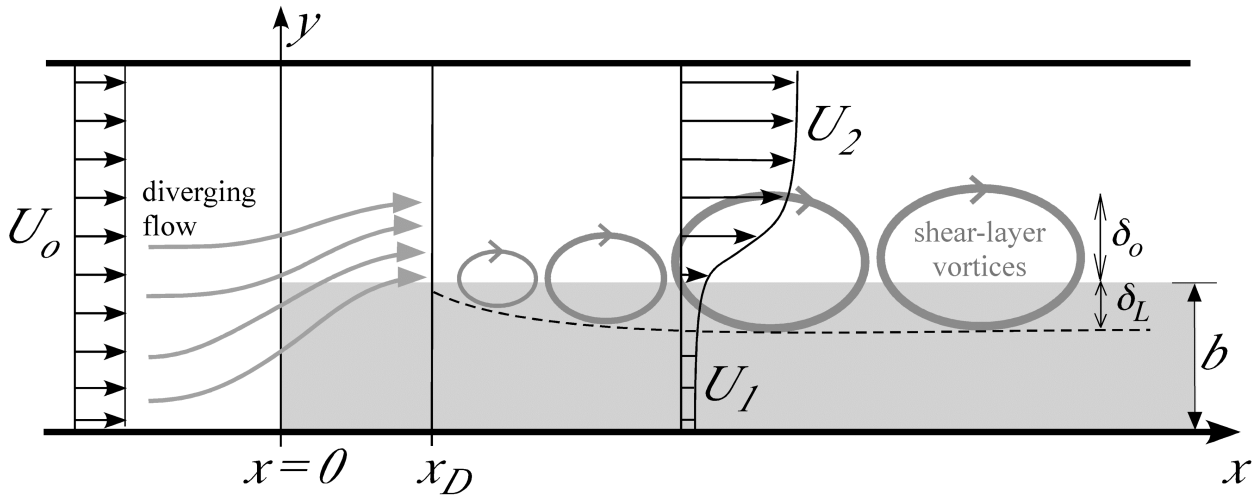

875
876 **Figure 3.** This is a top view of a channel with a long patch of emergent vegetation along the right
877 bank (grey shading). The width of the vegetation zone is b. The flow approaching from upstream
878 has uniform velocity U_o. The flow begins to diverge a distance b upstream and continues to
879 decelerate and diverge until distance x_D. After this point, a shear layer forms on the flow-parallel
880 edge, and shear-layer vortices form by Kelvin-Helmholtz instability. These vortices grow
881 downstream, but subsequently reach a fixed width and fixed penetration distance into the vegetation,
882 δ_v. Adapted from Zong and Nepf 2010.

883

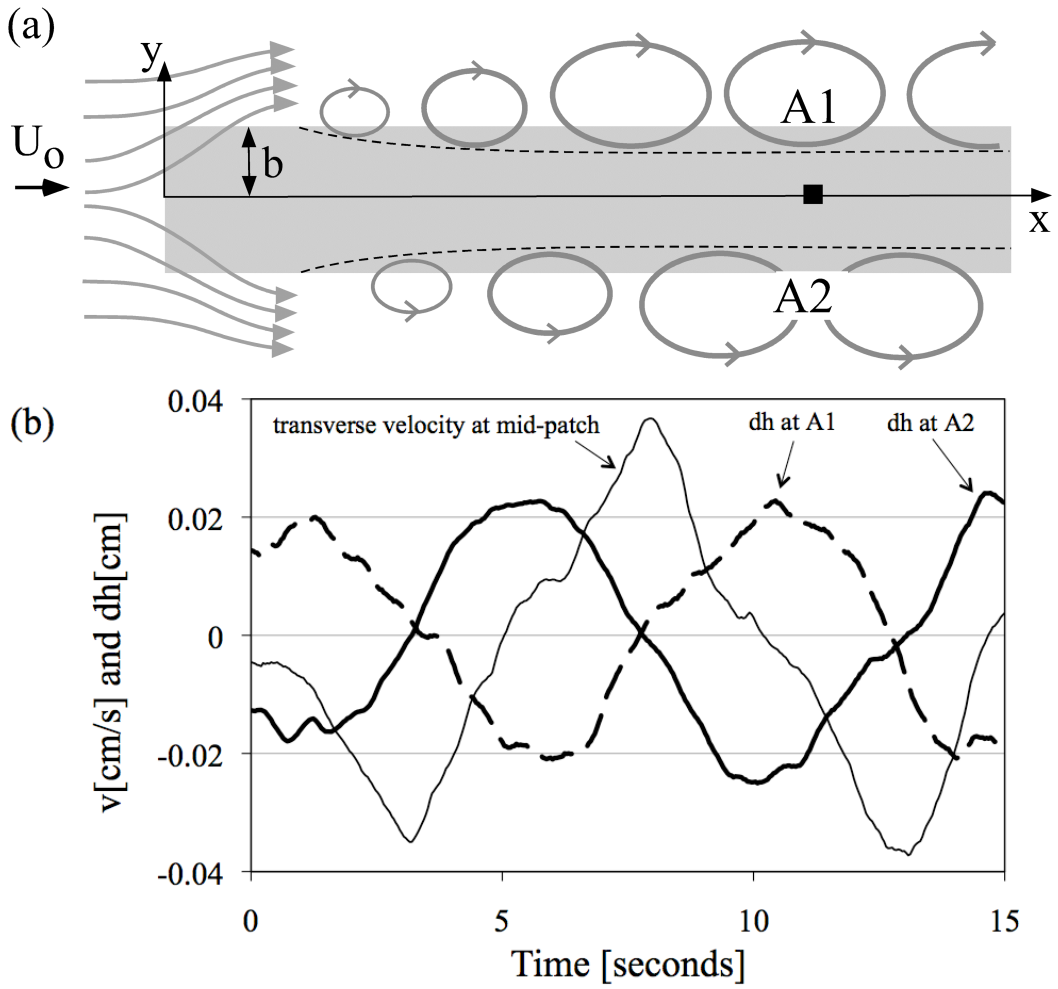

Figure 4. a) Top view of emergent vegetation with two flow-parallel edges. The patch width is 2*b*. The coherent structures on either side of the patch are out of phase. The passage of each vortex core is associated with a minimum in surface displacement, which is measured at the patch edges (A1 and A2). The velocity is measured mid-patch (square). b) Data measured with a patch of width b = 10 cm in a channel with flow U_o = 10 cms^{-1}. The patch centerline velocity is U_1 = 0.5 cms^{-1}. The surface displacements measured at A1 (heavy dashed line) and at A2 (heavy solid line) are a half cycle (π radians) out of phase. The resulting transverse pressure gradient imposed across the patch generates transverse velocity within the patch (thin line), which, as in a progressive wave, lags the lateral pressure gradient by a quarter cycle (π/2 radians). Adapted from Rominger and Nepf 2011.

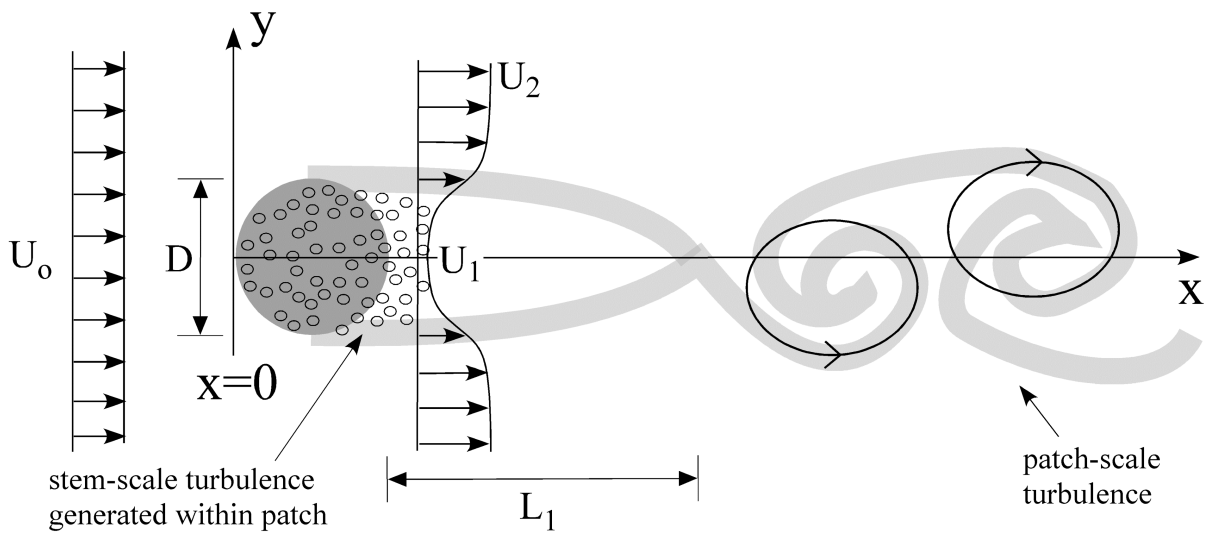

894

895 **Figure 5.** This is a top view of a circular patch of emergent vegetation with patch diameter *D*. The
896 upstream, open-channel velocity is U_O. Stem-scale turbulence is generated within the patch, but dies
897 out quickly behind the patch. Directly behind the patch is a steady wake region, with velocity U_1 at
898 the centerline. The flow in the steady wake blocks interaction between the shear-layers at the two
899 edges of the patch, which delays the onset of the patch-scale vortex street. Tracer (grey line)
900 released from the outermost edges of the patch come together at a distance L_1 downstream from the
901 patch, marking the end of the steady wake region.

902

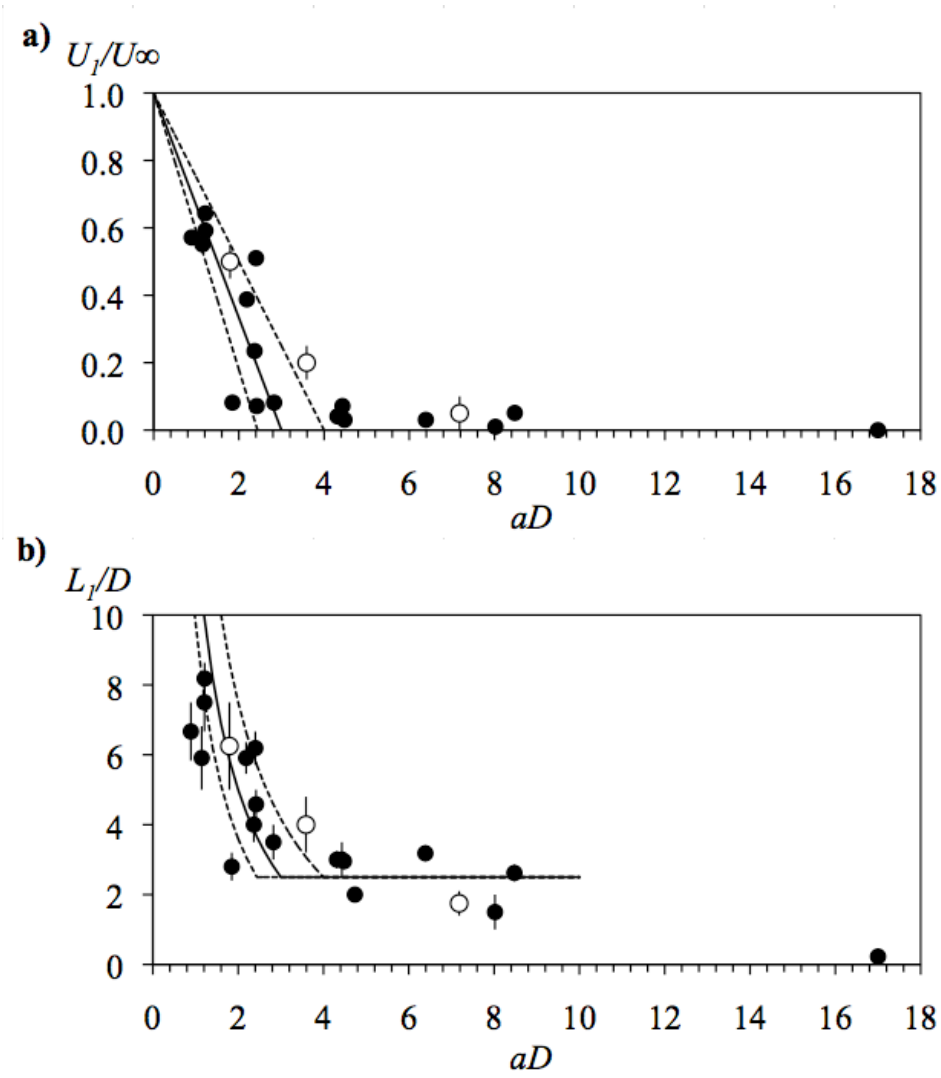

Figure 6. The flow blockage determines a) the velocity within the steady wake, U_1, and b) the length of the steady wake, L_1. a) For low flow blockage, the velocity ratio, U_1/U_o, fits a simple, linear relationship (eq. 14, shown with solid and dashed (S.D.) lines). For high flow blockage, the exit velocity is a small fraction of U_1, but non-zero, until $aD > 10$, at which point U_1 is indistinguishable from zero. b) For low flow blockage L_1 can be predicted from equations eq. (14) and (15), and becomes constant ($L_1/D = 2.5$) for high flow blockage. Model predictions are shown by black lines. Black circles measured with a circular array of circular cylinders (Chen at al. 2012). White circles measured with a square array of circular cylinders (Ball et al. 1996).

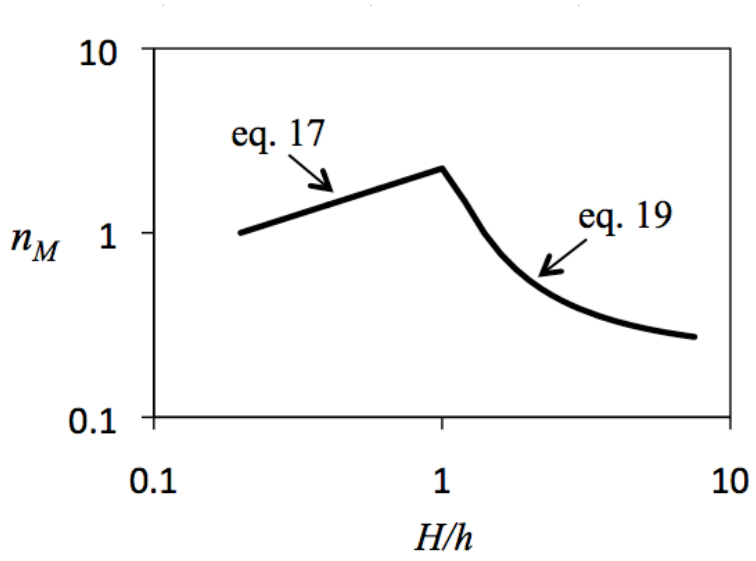

911

912 **Figure 7**. Mannings coefficient versus depth ratio (H/h). Most channel vegetation is flexible, so that
913 increasing velocity is associated with a decrease in vegetation height (h), i.e. $h \sim 1/V$, and the
914 previously noted non-linear trend of n_M with VR (e.g. Ree 1949) is captured by the trends of n_M with
915 H/h, as expressed through (17), for emergent conditions, and (19) for submerged conditions. Based
916 on Luhar and Nepf (2012).

917

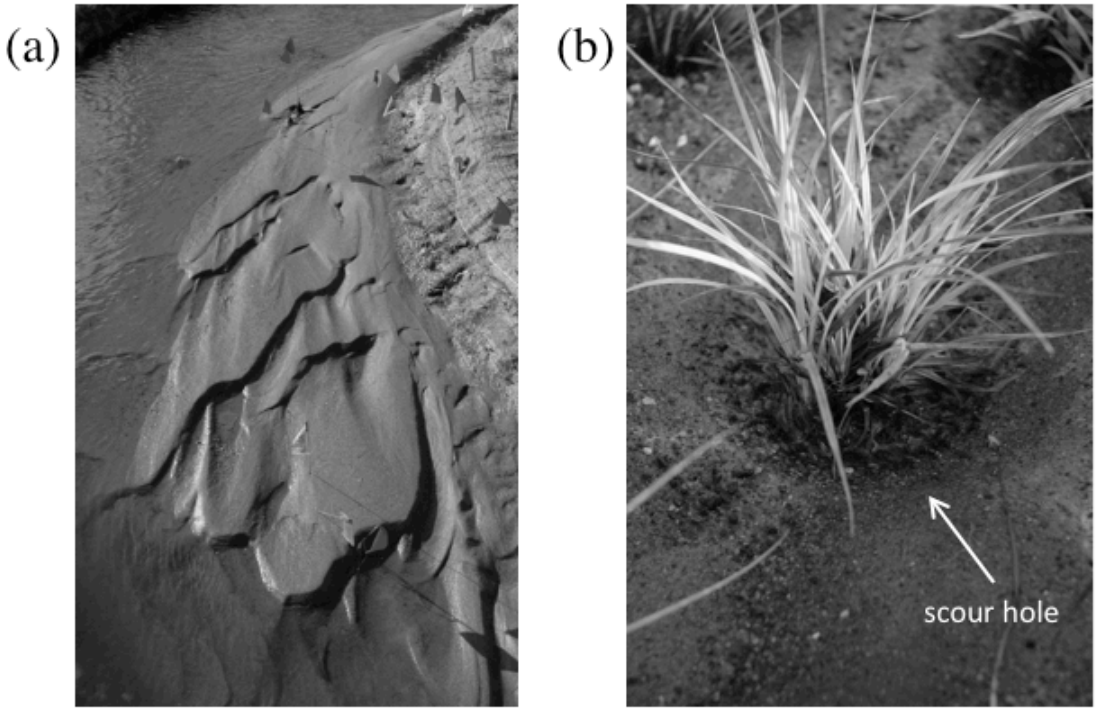

Figure 8. In a sand-bed river, the addition of vegetation to the point bars leads to a transition in bed form, from (a) migrating dunes to (b) a fixed patterns of scour associated with individual plants. Images taken by Jeff Rominger during the Outdoor StreamLab experiment at Saint Anthony Falls Laboratory 2008 (Rominger et al 2010).

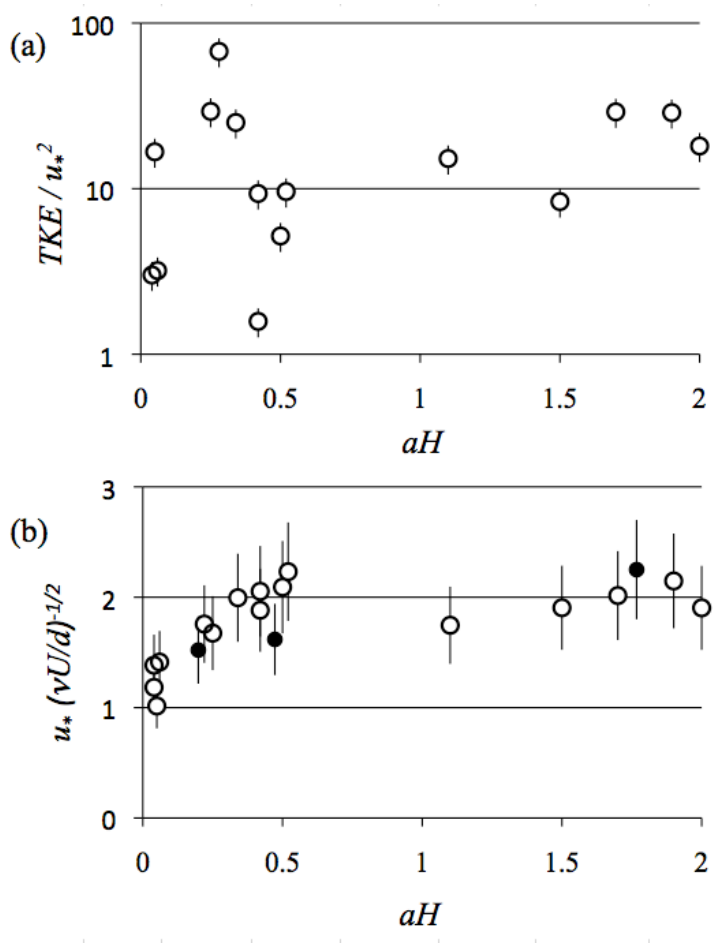

Figure 9. Measurements of bed stress in an array of emergent, rigid cylinders. Friction velocity estimated from spatial average of near-bed viscous stress, *i.e.* (20). White circles from F. Kerger (unpublished data). Black circles from Zavistoski (1992). a) Ratio of TKE to bed stress. Over a bare bed this ratio is 5 (*e.g.* Stapleton and Huntley 1995). b) Bed friction velocity normalized by bed stress estimator, as in (22). For sufficiently dense array, the ratio has a constant value.

928 Literature Cited

929 Abdelrhman, M. (2007). Modeling coupling between eelgrass Zostera marina and water flow. *Mar Ecol-Prog*
930 *Ser* 338, 81–96, doi:10.3354/meps338081.

931 Abt, S., Clary W., Thornton, C. (1994). Sediment deposition and entrapment in vegetated streambeds. *J. Irrig*
932 *Drain E-ASCE* 120 (6), 1098-1110.

933 Ackerman, J. (1997). Submarine pollination in the marine angiosperm *Zostera marina*. *Am J Bot* 84 (8),
934 1110-1119.

935 Ackerman, J. (2000). Abiotic pollen and pollination: ecological, functional, and evolutionary perspectives.
936 *Plant Syst Evol* 222, 167-185.

937 Afzalimehr, H., Dey, S. (2009). Influence of bank vegetation and gravel bed on velocity and Reynolds stress
938 distributions. *Int. J. Sediment Res*. 24 (2), 236-246.

939 Alben, S., Shelley, M., Zhang, J. (2002). Drag reduction through self-similar bending of a flexible body.
940 *Nature* 420, 479-81.

941 Bal, K., Struyf, E., Vereecken, H., Viaene, P., De Doncker, L., de Deckere, E., Mostaert, F., Meire, P. (2011).
942 How do macrophyte distribution patterns affect hydraulic resistances? *Ecol Eng* 37 (3), 529–33.

943 Ball, B. J., Stansby, P. K., Alliston, N. (1996). Modeling shallow water flow around pile groups. *PI Civil*
944 *Eng-Water*, *118*, 226-236, doi: 10.1680/iwtme.1996.28987.

945 Baptist, M.J., Babovic V., Uthurburu J.R., Keijzer M., Uittenbogaard R.E., Mynett A., Verwey, A. (2007). On
946 inducing equations for vegetation resistance. *J Hydraulic Res.* 45(4), 435–50.

947 Belcher, S., Jerram, N., Hunt, J. (2003). Adjustment of a turbulent boundary layer to a canopy of roughness
948 elements. *J Fluid Mech.* 488, 369-98.

949 Bennett S., Pirim T., Barkdoll B. (2002). Using simulated emergent vegetation to alter stream flow direction
950 within a straight experimental channel. *Geomorphology* 44, 115–126.

951 Bennett, S., Wu, W., Alonso, C., Wang, S. (2008). Modeling fluvial response to in-stream woody vegetation:
952 implications for stream corridor restoration. *Earth Surf Proce Land* 33:890-909.

953 Bernhardt, E., M. Palmer, J. Allan, and the National River Restoration Science Synthesis Working Group.
954 (2005). Restoration of U.S. rivers: A national synthesis. *Science* 308, 636–637.

955 Boudreau, B. and B. Jorgensen. (2001). *The Benthic Boundary Layer: Transport and Biogeochemistry*. Oxford;
956 New York: Oxford University Press.

957 Bos, A., Bouma, T., de Kort, G., van Katwijk, M. (2007). Ecosystem engineering by annual intertidal seagrass
958 beds: sediment accretion and modification. *Estuar. Coast Shelf S.*, 74, 344-348.

959 Bouma, T., van Duren, L., Temmerman, S., Claverie, T., Blanco-Garcia, A., Ysebaert, T., Herman, P. (2007).
960 Spatial flow and sedimentation patterns within patches of epibenthic structures: Combining field, flume
961 and modelling experiments, *Cont. Shelf Res.*, 27, 1020–1045, doi:10.1016/j.csr.2005.12.019.

962 Bouma, T., Friedrichs, M., van Wesenbeeck, B., Temmerman, S., Graf, G., Herman, P. (2009). Density-
963 dependent linkage of scale-dependent feedbacks: a flume study on the intertidal macrophyte Spartina
964 anglica. *Oikos*, 118, 260-268, doi: 10.1111/j.1600-0706.2008.16892.x.
965 Brampton AH. (1992). Engineering significance of British saltmarshes. *In* Saltmarshes: Morphodynamics,
966 Conservation, and Engineering Significance, ed. JRL Allen, K Pye, Cambridge University Press, p. 115–
967 122.
968 Bradley K., Houser C. (2009). Relative velocity of seagrass blades: Implications for wave attenuation in low-
969 energy environments. *J Geophys. Res*., 114: F01004.
970 Braudrick, C.A., Dietrich, W.E., Leverich, G.T., Sklar, L.S. (2009). Experimental evidence for the conditions
971 necessary to sustain meandering in coarse-bedded rivers. *PNAS*, 106(40), 16936-16941.
972 Brookshire, E., K. Dwire (2003). Controls on patterns of coarse organic particle retention in headwater
973 streams. *J.N. Am. Benth. Soc.,* 22, 17–34.
974 Burke R, Stolzenbach K. (1983). Free surface flow through salt marsh grass. *Technical Report*. Massachusetts
975 Institute of Technology, Sea Grant, 83-16, Cambridge, MA.
976 Carpenter SR, Lodge DM. (1986). Effects of submersed macrophytes on ecosystem processes. *Aquat Bot* 26,
977 341-70.
978 Castro, I.P. (1971). Wake characteristics of two-dimensional perforated plates normal to an air-stream. *J.*
979 *Fluid Mech.*, 46, 599-609, doi:10.1017/S0022112071000727.
980 CBEC, Chesapeake Bay Executive Council (2003) *Expanded Riparian Forest Buffer Goals*. Directive 03-01.
981 Annapolis, Maryland 21403
982 Celik, A., Diplas, P., Dancey, C., Valyrakis, M. (2010). Impulse and particle dislodgement under turbulent
983 flow conditions. *Phys. Fluids* 22, 046601, doi:10.1063/1.3385433.
984 Chambers, P., Prepas, E. (1994). Nutrient dynamics in riverbeds: the impact of sewage effluent and aquatic
985 macrophytes, *Water Res,* 28, 453-464.
986 Chambert, S., James C. (2009), Sorting of seeds by hydrochory. *River Res. Appl*., 25, 4861,
987 doi:10.1002/rra.1093.
988 Chen, D., Jirka, G. H. (1995). Experimental study of plane turbulent wakes in a shallow water layer. *Fluid*
989 *Dyn Res.* 16 (1), 11–41.
990 Chen, Z., A. Ortiz, L. Zong and H. Nepf. (2012). The wake structure behind a porous obstruction with
991 implications for deposition near a finite patch of emergent vegetation. Submitted to *Water Resour Res.*
992 Cheng N. (2011) Representative roughness height of submerged vegetation. *Water Resour Res*. 47:W08517.
993 Clarke, S. (2002). Vegetation growth in rivers: influences upon sediment and nutrient dynamics. *Prog Phys*
994 *Geog* 26(2), 159-172, doi:10.1191/0309133302pp324ra

995 Costanza, R., d'Arge, R., de Groot, R., Farber, S., Grasso, M., Hannon, B., Limburg, K., Naeem, S., O'Neill,
996 R.V., Paruelo, J., Raskin, R.G., Sutton, P., van den Belt, M. (1997). The value of the world's ecosystem
997 services and natural capital. *Nature* 387, 253-60.
998 Cotton, J., Wharton, G., Bass, J., Heppell, C., Wotton, R. (2006). The effects of seasonal changes to in-
999 stream vegetation cover on patterns of flow and accumulation of sediment. *Geomorphology* 77, 320–334.
1000 de Langre E. (2008). Effects of wind on plants. *Ann Rev Fluid Mech*, 40, 141-68,
1001 doi:10.1146/annurev.fluid.40.111406.102135
1002 Denny, M. and L. Roberson. (2002). Blade motion and nutrient flux to the kelp, Eisenia arborea. *Biol. Bull*.
1003 203, 1-13.
1004 Defina, A., Bixio, A. (2005). Mean flow and turbulence in vegetated open channel flow. *Water Resour. Res.* 41,
1005 W07006, doi:10.1029/2004WR003475.
1006 Defina, A. and P. Peruzzo (2010). Floating particle trapping and diffusion in vegetated open channel flow.
1007 *Water Resour. Res*., 46, W11525, doi:10.1029/2010WR009353.
1008 Dijkstra J, Uittenbogaard R. (2010). Modeling the interaction between flow and highly flexible aquatic
1009 vegetation. *Water Resour Res*. 46, W12547, doi:10.1029/2010WR009246
1010 Eckman J. (1990). A model of passive settlement by planktonic larvae onto bottoms of differing roughness.
1011 *Limnol Oceanogr* 35, 887-901.
1012 Escauriaza, C., Sotiropoulos, F. (2011). Initial stages of erosion and bed form development in a turbulent flow
1013 around a cylindrical pier. *J. Geo. Res*., 116, F03007, doi:10.1029/2010JF001749.
1014 Feurer, D., Bailly, J. and Puech, C. (2008a) Measuring depth of a clear, shallow, gravel-bed river by through-
1015 water photogrammetry with small format cameras and ultra light aircrafts. In *Geophysical Research*
1016 *Abstracts* 10, European Geosciences Union (EGU) General Assembly, 14–18 April, Vienna.
1017 Feurer, D. Bailly, J.-P., Puech, C., Le Coarer, Y. and Viau, A. (2008b). Very high-resolution mapping of
1018 river-immersed topography by remote sensing. Prog. In Physical Geography, 32(4);403-419.
1019 Finnigan J. (2000). Turbulence in plant canopies. *Ann. Rev. Fluid Mech*. 32:519-71
1020 Finnigan, J., Shaw, R., Patton, E. (2009). Turbulence structure above a vegetation canopy. *J. Fluid Mech*.
1021 637:387-424
1022 Fitzmaurice L., Shaw, R., Paw, U. K.T., Patton E. (2004). Three-dimensional scalar microfronts in a large-
1023 eddy simulation of vegetation canopy flow. *Bound.-Layer Met*. 112:107–27.
1024 Folkard, A. (2010). Vegetated flows in their environmental context: a review, *Proc. of Inst. of Civil Eng. –*
1025 *Eng. & Comp. Mechanics*, doi: 10.1680/eacm.8.00006.
1026 Folkard, A. (2011). Flow regimes in gaps within stands of flexible vegetation: laboratory flume simulations,
1027 *Env. Fluid Mech*, 11:289-386, doi: 10.1007/s10652-010-437 9197-5.
1028 Fonseca, M., Zieman, J., Thayer, G. (1983). The role of current velocity in structuring eelgrass (*Zostera*

1029 *marina L.*) meadows. *Estuar. Coast Shelf Sci. 17* (4), 367-380, doi:10.1016/0272-7714(83)90123-3.
1030 Gambi, M., Nowell, A., Jumars, P. (1990). Flume observations on flow dynamics in *Zostera marina*
1031 (eelgrass) beds. *Mar. Ecol. Prog. Ser.* 61:159-69
1032 Gao W, Shaw R, Paw U KT. (1989). Observation of organized structure in turbulent flow within and above a
1033 forest canopy. *Bound.-Layer Meteorol.* 47:349–77
1034 Gaylord, B., Reed, D., Washburn, L., Raimondi, P. (2004). Physical-biological coupling in spore dispersal of
1035 kelp forest macroalgae. *J. Mar. Syst*. 49:19-39
1036 Ghisalberti, M. (2000). *Mixing Layers and coherent structures in vegetated aquatic flows*. *MS Thesis*.
1037 Massachusetts Institute of Technology
1038 Ghisalberti, M. (2005). Momentum and Scalar Transport in Vegetated Shear Flows. *PhD Thesis*.
1039 Massachusetts Institute of Technology
1040 Ghisalberti, M. (2009). Obstructed shear flows: similarities across systems and scales. *J. Fluid Mech*. 641, 51-
1041 61
1042 Ghisalberti, M., Nepf, H. (2002). Mixing layers and coherent structures in vegetated aquatic flow. *J. Geophys.*
1043 *Res.*, 107(C2), 10.1029/2001JC000871
1044 Ghisalberti, M., Nepf H. (2004). The limited growth of vegetated shear -layers. *Water Resour. Res.* 40,
1045 W07502, doi:10.1029/2003WR002776
1046 Ghisalberti M, Nepf, H. (2005). Mass Transfer in Vegetated Shear Flows. *Env. Fluid Mech*. 5(6): 527-51,
1047 doi10.1007/s10652-005-0419-1
1048 Ghisalberti, M., Nepf, H. (2006). The structure of the shear layer over rigid and flexible canopies. *Env. Fluid*
1049 *Mech*. 6(3):277-301, doi10.1007/s10652-006-0002-4
1050 Ghisalberti, M., Nepf, H. (2009). Shallow flows over a permeable medium: the hydrodynamics of submerged
1051 aquatic canopies. *Transport Porous Med.* 78:385-402, doi:10.1007/s11242-009-9434-x
1052 Gosselin, F., deLangre, E., Machado-Almeida, B. (2010). Drag reduction of flexible plates by reconfiguration,
1053 *J. Fluid Mech*. 650:319-41.
1054 Gourlay, M. (1970). Discussion of: Flow resistance in vegetated channels, by Kouwenm Unny, and Hill. *J.*
1055 *Irrig Drainage E-ASCE*, 96(IR3), 351-357.
1056 Green, E.P, Short, F,T. (2003). *World Atlas of Seagrasses*, Univ. California Press, 310 pp.
1057 Green J. (2005a). Further comment on drag and reconfiguration of macrophytes. *Freshwater. Biol*. 50, 2162-
1058 66.
1059 Green, J. (2005b). Comparison of blockage factors in modelling the resistance of channels containing
1060 submerged macrophytes, *River Res. Applic.*, 21, 671-686
1061 Green, J., (2006). Effect of macrophyte spatial variability on channel resistance, *Adv Water Resour.* 29, 426-
1062 438

1063 Gray, W.G., Lee, P.C.Y. (1977). On the theorems for local volume averaging of multiphase systems. *Inter. J.*
1064 *Multiphase Flow*. 3(4), 333-40
1065 Gurnell, A., van Oosterhout, M., de Vlieger, B., Goodson, J. (2006). Reach-scale interactions between aquatic
1066 plants and physical habitat: River Frome, Dorset. *River Res. App*. 22(6): 1535-1467.
1067 Harvey, J., Conklin, M., Koelsch, R. (2003). Predicting changes in hydrologic retention in an evolving semi-
1068 arid alluvial stream, *Adv. Water. Resour*., *26*, 939-950.
1069 Heritage, G., Milan, D. (2009). Terrestrial laser scanning of grain roughness in a gravel-bed river.
1070 *Geomorphology*, 113(2):1-11.
1071 Huang, Y-H., Saiers, J., Harvey, J., Noe, G., Mylon, S. (2008). Advection, dispersion, and filtration of fine
1072 particles within emergent vegetation of the Florida Everglades. *Water. Resour. Res*. 44, W04408,
1073 doi:10.1029/2007WR006290.
1074 Huang, I., Rominger, J., Nepf, H. (2011). The motion of kelp blades and the surface renewal model. *Limnol.*
1075 *Oceanogr*. 56(4): 1453-14562, doi:10.4319/lo.2011.56.4.1453
1076 Hurd, C., Harrison, P., Druehl, L. (1996). Effect of seawater velocity on inorganic nitrogen uptake by
1077 morphologically distinct forms of the giant kelp *Macrocystis inregrifolia* from wave-sheltered and
1078 exposed sites. *Mar. Biol*., 126, 205-214.
1079 Hurd, C., Stevens, C., Laval, B., Lawrence, G., Harrison, P. (1997). Visualization of seawater flow around
1080 morphologically distinct forms of the giant kelp *Macrocystis inregrifolia* from wave-sheltered and
1081 exposed sites. *Limnol. Oceanogr*, 41(1), 156-163.
1082 Hurd, C.L. (2000). Water motion, marine macroalgal physiology, and production. *J. Phycol*. 36, 453-72.
1083 Huthoff, F., Augustijn, D.C.M., Hulscher, S.J.M.H. (2007) Analytical solution of the depthaveraged flow
1084 velocity in case of submerged rigid cylindrical vegetation. *Water Resour Res.* 43(6), W06413.
1085 Ishikawa, Y., Sakamoto, T., Mizuhara, K. (2003). Effect of density of riparian vegetation on effective tractive
1086 force. *J Forest Res*. 8(4), 235-246.
1087 Jordanova, A., James, C. S. (2003) Experimental Study of Bed Load Transport through Emergent Vegetation.
1088 *J. Hydraul. Eng*. ASCE, 129 (6): 474-478.
1089 Julien, P. (2010). *Erosion and Sedimentation.* 2nd ed., Cambridge University Press. Cambridge, United
1090 Kingdom.
1091 Kaimal, J., Finnigan, J. (1994). *Atmospheric Boundary Layer Flows: Their Structure and Measurement*.
1092 Oxford University Press, Oxford, United Kingdom.
1093 Kays, W., Crawford, M. (1993). *Convective Heat and Mass Transfer*. 3rd ed. McGraw-Hill, New York.
1094 Kemp, J., Harper, D., Crosa, G. (2000). The habitat-scale ecohydraulics of rivers. *Ecol. Eng.*, 16, 17-29.
1095 Kobayashi N., Raichle A., Asano T. (1993). Wave attenuation by vegetation. *J. Waterw Port C Oce-ASCE*,
1096 119:30-48

1097 Koch E.W. (1994). Hydrodynamics, diffusion-boundary layers and photosynthesis of the seagrasses,
1098 *Thalassia testudinum* and *Cymodocea nodosa*. *Mar Biol*, 118, 767-76.
1099 Koch, E. (2001). Beyond Light: Physical, Geological, and Geochemical Parameters as Possible Submersed
1100 Aquatic Vegetation Habitat Requirements, *Estuaries* 24(1), 1–17.
1101 Koehl, M., Alberte, R. (1988). Flow, flapping, and photosynthesis of *Nereocystis luetkeana*: a functional
1102 comparison of undulate and flat blad morphology. *Mar. Biol*. 99, 435-444
1103 Kouwen, N., T. Unny (1973). Flexible Roughness in Open Channels, *J. Hyd.* 99(HY5), 713-728.
1104 Kouwen, N. (1990). Modern Approach to Design of Grassed Channels, *J. Irrig. and Drain*, 118, 733-743.
1105 Kundu, P., Cohen, I. (2002). *Fluid Mechanics*. 2nd ed. Academic Press.
1106 Lacy, J., Whllie-Echeverria, S. (2011). The influence of current speed and vegetation density on flow
1107 structure in two macrotidal eelgrass canopies. *Limnol Oceanogr: Fluids and Environments*, 1, 38–55 DOI
1108 10.1215/21573698-1152489.
1109 Larsen, L., Harvey, J. (2011). Modeling of hydroecological feedbacks predicts distinct classes of landscape
1110 pattern, process, and restoration potential in shallow aquatic ecosystems. *Geomorphology* 126:279–296,
1111 doi:10.1016/j.geomorph.2010.03.015.
1112 Larsen, L., J. Harvey (2010). How vegetation and sediment transport feedbacks drive landscape change in the
1113 Everglades. *Am. Nat.* 176, E66–E79.
1114 Larsen, L., Harvey, J., Crimaldi, J. (2009). Predicting bed shear stress and its role in sediment dynamics and
1115 restoration potential of the Everglades and other vegetated flow systems. *Ecol. Eng*. 35:1773-1785.
1116 Lawler, D. (2008). Advances in the continuous monitoring of erosion and deposition dynamics:
1117 Developments and applications of new PEEP-3T system. *Geomorphology*, 93(1-2):17-39.
1118 Lawson, S., McGlathery, K., Wiberg, P. (2012). Enhancement of sediment suspension and nutrient flux by
1119 benthic macrophytes at low biomass. *Mar. Ecol. Prog. Ser*. 448, 259-270, doi: 10.3354/meps09579.
1120 Li, S., Millar, R. (2010). A two-dimensional morphodynamic model of gravel-bed river with floodplain
1121 vegetation. *Earth Surf. Proc. Land*. 36, 190-202.
1122 Lightbody, A., Nepf, H. (2006). Prediction of velocity profiles and longitudinal dispersion in emergent salt
1123 marsh vegetation. *Limnol. Oceanogr.* 51(1), 218-28.
1124 Lightbody, A., Avener, M., Nepf. H. (2008). Observations of short-circuiting flow paths within a constructed
1125 treatment wetland in Augusta, Georgia, USA. *Limnol. Oceanogr.,* 53(3), 1040-1053.
1126 Liu, D., Diplas, P., Fairbanks, J., Hodges, C. (2008). An experimental study of flow through rigid vegetation.
1127 *J. Geophys. Res*., 113, F04015, doi:10.1029/2008JF001042.
1128 Lopez, F., Garcia, M., (1998). Open-channel flow through simulated vegetation: suspended sediment
1129 transport modeling. *Water Resour. Res*. 34(9), 2341-52.

1130 Lopez, F., Garcia, M. (2001). Mean flow and turbulence structure of open-channel flow through non-
1131 emergent vegetation. *J. Hydraul. Res*. 127, 392-402.
1132 Lowe R., Koseff, J., Monismith S. (2005). Oscillatory flow through submerged canopies: 1. Velocity
1133 structure. *J. Geophys. Res.,* 110*,* (C10016), doi:10.1029/2004JC002788.
1134 Luhar, M., Rominger, J., Nepf, H. (2008). Interaction between flow, transport and vegetation spatial structure.
1135 *Env. Fluid Mech.* 8(5-6), 423-39.
1136 Luhar, M., Nepf. H. (2011). Flow induced reconfiguration of buoyant and flexible aquatic vegetation. *Limnol.*
1137 *Oceanogr*, 56(6), 2003-2017, doi:10.4319/lo.2011.56.6.2003
1138 Luhar, M., Nepf, H. (2012). From the blade scale to the reach scale: a characterization of aquatic vegetative
1139 drag. Accepted. *Adv. Water. Resour*.
1140 Mars, M., Kuruvilla, M., Goen, H. (1999). The role of submergent macrophyte *triglochin huegelii* in domestic
1141 greywater treatment. *Ecol. Eng.*, 12, 57-66.
1142 Meijer, D.G., van Velzen, E.H. (1998). Prototype-scale flume experiments on hydraulic roughness of
1143 submerged vegetation. *Technical report*.
1144 Mendez F., Losada I. (2004). An empirical model to estimate the propagation of random breaking and
1145 nonbreaking waves over vegetation fields. *Coast Eng*., 51:103-118.
1146 Mertes, L. (2002). Remote sensing of riverine landscapes. *Freshwater Biol* 47, 799–816.
1147 Mitsch, W.J, Gosselink, J.G. (1986). *Wetlands*. 2nd Ed. Van Nostrand Reinhold, 712pp
1148 Moore KA. (2004). Influence of seagrasses on water quality in shallow regions of the lower Chesapeake Bay,
1149 *J. Coast. Res.*, 20 (Special Issue), 162-78.
1150 Mudd, S., D'Alpaos, A., Morris, J. (2010). How does vegetation affect sedimentation on tidal marshes?
1151 Investigating particle capture and hydrodynamic controls on biologically mediated sedimentation. *J.*
1152 *Geophys. Res*. 110(F03029):14. doi:10.1029/2009JF001566.
1153 Murphy, E., Ghisalberti, M., Nepf, H. (2007). Model and laboratory study of dispersion in flows with
1154 submerged vegetation, *Water Resour. Res*., 43, W05438, doi:10.1029/2006WR005229.
1155 Naden, P., Rameshwaran, P., Mountford, O., Robertson, C. (2006). The influence of macrophyte growth,
1156 typical of eutrophic conditions, on river flow velocities and turbulence production. *Hydrol. Proc.*
1157 20:3915-38.
1158 Nicolle, A., Eames, I. (2011). Numerical study of flow through and around a circular array of cylinders, *J.*
1159 *Fluid Mech.*, *679*, 1-31, doi:10.1017/jfm.2011.77.
1160 National Research Council (2002). *Riparian Areas: Functions and Strategies for Management*. National
1161 Academy Press, Washington, D.C.
1162 Neary, V.S. (2003) Numerical solution of fully developed flow with vegetative resistance. *J Eng Mech ASCE*
1163 129(5), 558–63.

1164 Nellemann, C., Corcoran, E., Duarte, C. M., Valdés, L., De Young, C., Fonseca, L., Grimsditch, G. (Eds).
1165 (2009). *Blue Carbon. A Rapid Response Assessment. United Nations Environment Programme*, Arendal,
1166 Norway.
1167 Nepf, H. (1999). Drag, turbulence, and diffusion in flow through emergent vegetation. *Water Res. Res.*
1168 35:479-89.
1169 Nepf H. (2012). Flow over and through biota. In: Treatise on Estuarine and Coastal Science. ed. E Wolanski,
1170 D McLusky, Elsevier Inc., San Diego.
1171 Nepf, H. (2012). Flow and transport in regions with aquatic vegetation. *Ann. Rev. of Fluid Mech*., 44:123-42,
1172 doi: 10.1146/annurev-fluid-120710-101048.
1173 Nepf, H., Ghisalberti, M., White, B., Murphy, E.. (2007). Retention time and dispersion associated with
1174 submerged aquatic canopies, *Water Res. Res*., 43, W04422, doi:10.1029/2006WR005362.
1175 Nepf, H. (2000). Reply to Comment: Drag, turbulence and diffusivity in flow through emergent vegetation.
1176 *Water Resour. Res.*, 36(7): 1987-1988.
1177 Nepf, H., Sullivan, J., Zavistoski, R. (1997). A model for diffusion within an emergent plant canopy. *Limnol.*
1178 *Oceanogr.* 42(8):85-95.
1179 Nepf, H., Vivoni, E. (2000). Flow structure in depth-limited, vegetated flow. *J. Geophys. Res.* 105(28):547-57.
1180 Neumeier, U. (2007). Velocity and turbulence variations at the edge of saltmarshes, *Cont. Shelf Res.*,
1181 27:1046-1059, doi: 10.1016/j.csr.2005.07.009.
1182 Nezu, I., Onitsuka, K. (2001). Turbulent structures in partly vegetated open-channel flows with LDA and PIV
1183 measurements. *J. Hydraul Res.*, 39(6):629-642.
1184 Nezu, I., Rodi, W. (1986). Open-channel flow measurements with a laser Doppler anemometer, *J. Hydraulic*
1185 *Eng.- ASCE*, 112(5):335-355.
1186 Nikora, V., McEwan, I., McLean, S., Coleman, S., Pokrajac, D., Walters, R. (2007). Double-averaging concept
1187 for rough-bed open-channel and overland flows: theoretical background. *J. of Hydraulic Engineering*,
1188 ASCE, 133(8):873-883.
1189 Nikora, N., Nikora, V. (2007). A viscous drag concept for flow resistance in vegetated channels. [CD-ROM]
1190 Proceedings of the 32nd IAHR Congress, Venice, 1-6 July.
1191 Nikora, V., Lamed, S., Nikora, N., Debnath, K., Cooper, G., Reid, M. (2008) Hydraulic resistance due to
1192 aquatic vegetation in small streams: field study. *J Hydraul Eng* ASCE 134(9), 1326–32.
1193 Nilsson, C., Reidy, C., Dynesius, M., Revenga, C. (2005). Fragmentation and flow regulation of the world's
1194 large river systems, *Science*, 308, 405-408.
1195 Nino, Y., Garcia, M. (1996). Experiments on particle-turbulence interactions in the near-wall region of an open
1196 channel flow: implications for sediment transport. *J. Fluid Mech*., 326, 285-319.

1197 Noe, G., Hupp, C. (2009). Retention of riverine sediment and nutrient loads by coastal plain floodplains.
1198 *Ecosystems*, 12, 728-746.
1199 Okamoto T, Nezu I. (2009). Turbulence structure and monami phenomena in flexible vegetated open-channel
1200 flows. *J. Hydraulic Res*., 47(6), 798-810.
1201 Oki, T., Kanae, S. (2006). Global hydrological cycles and world water resources, *Science*, 313, 1068-1072.
1202 Othman, M.A. (1994). Value of mangroves in coastal protection. *Hydrobiologia*, 285, 277-282.
1203 Palmer M., Bernhardt E. (2006). Hydroecology and river restoration: ripe for research and synthesis. *Water*
1204 *Resour Res* 42: W03S07. doi: 10.1029/2005WR004354.
1205 Papanicolaou, A., Diplas, P., Evaggelopoulos, N., Fotopoulos, S. (2002). Stochastic incipient motion criterion
1206 for spheres under various bed packing conditions, *J. Hydrol. Eng*. 128, 369-380.
1207 Plew, D., G. Cooper, and F. Callaghan (2008). Turbulence induced forces in a freshwater macrophyte canopy,
1208 *Water Resour. Res*., 44, W02414, doi:10.1029/2007WR006064.
1209 Poggi, D., Porporato, A,, Ridolfi, L., Albertson, J., Katul, G. (2004a). The effect of vegetation density on
1210 canopy sub-layer turbulence. *Bound. Lay. Met.* 111:565-87.
1211 Poggi, D,, Katul, G., Albertson, J., (2004b). A note on the contribution of dispersive fluxes to momentum
1212 transfer within canopies. *Bound. Lay. Met.* 111:615-21.
1213 Poggi, D., Krug, C., Katul, G.G. (2009) Hydraulic resistance of submerged rigid vegetation derived from
1214 first-order closure models. Water Resour Res 45, W10442.
1215 Pollen, N., Simon, A. (2005). Estimating the mechanical effects of riparian vegetation on stream bank stability
1216 using a fiber bundle model. *Water Resour. Res.*, 41, W07025, doi:10.1029/2004WR003801.
1217 Pollen-Bankhead, N., Simon, A. (2010). Hydrologic and hydraulic effects of riparian root networks on
1218 streambank stability: Is mechanical root-reinforcement the whole story? *Geomorphology*, 116(3-4), 353-
1219 362.
1220 Raupach, M., Shaw, R. (1982). Averaging procedures for flow within vegetation canopies. *Bound. Lay. Met.*
1221 *22*, 79-90.
1222 Raupach, M. (1992). Drag and drag partition on rough surfaces Bound.-Lay. Meteorol., 60(4), 375-395
1223 Raupach, M, Finnigan, J., Brunet, Y. (1996). Coherent eddies and turbulence in vegetation canopies: The
1224 mixing-layer analogy. *Bound. Lay. Met*. 60:375-95.
1225 Ree, W.O. (1949) Hydraulic characteristics of vegetation for vegetated waterways. *Agr Eng* 30:184–9.
1226 Righetti, M., Armanini, A. (2002). Flow resistance in open channel flows with sparsely distributed bushes. *J. of*
1227 *Hydrology*, 269 (1-2):55-64.
1228 Righetti, M. (2008). Flow analysis in a channel with flexible vegetation using double-averaging method. *Acta*
1229 *Geophysica*, 56(3), 801-823, doi: 10.2478/s11600-008-0032-z

1230 Rominger, J., Lightbody, A., Nepf, H. (2010). Effects of added vegetation on sand bar stability and stream
1231 hydrodynamics. *J. Hydraul. Eng.* 136 (12), 994-1002.
1232 Rominger, J., Nepf, H. (2011). Flow adjustment and interior flow associated with a rectangular porous
1233 obstruction. *J. Fluid. Mech*., 680:636–659, doi:10.1017/jfm.2011.199.
1234 Rowinski, P.M., Kubrak, J. (2002) A mixing-length model for predicting vertical velocity distribution in
1235 flows through emergent vegetation. *Hydrol Sci J* 47(6):893–904.
1236 Rowinski, P.M., Aberle, J., Mazurczyk, A. (2005). Shear velocity estimation in hydraulic research. *Acta*
1237 *Geophysica Polonica*, 53(4), 567-584.
1238 Sand-Jensen, K. (1998). Influence of submerged macrophytes on sediment composition and near-bed flow in
1239 lowlands streams, *Freshwater Biol*, 39:663-679.
1240 Sand-Jensen K. (2003). Drag and reconfiguration of freshwater macrophytes. *Freshwater Biol*. 48:271-83
1241 Sand-Jensen, K., Pedersen, M. L. (2008). Streamlining of plant patches in streams. Freshwater Biol. 53, 714–
1242 726.
1243 Sand-Jensen, K., Madsen, T.V. (1992). Patch dynamics of the stream macrophyte, Callitriche cophocarpa,
1244 *Freshwater Biol.*, *27*, 277-282, doi:10.1111/j.1365-2427.1992.tb00539.x.
1245 Schnauder, I., Moggridge, H. (2009), Vegetation and hydraulic-morphological interactions at the individual
1246 plant, patch and channel scale. *Aquat. Sci*., *71*, 318-330, doi 10.1007/s00027-009-9202-6.
1247 Schoneboom,T., Aberle, J., Dittrich, A. (2010) CHydraulic resistance of vegetated flows: Contribution of bed
1248 shear stress and vegetative drag to total hydraulic resistance. In River Flow 2010, Braunschweig,
1249 Germany (ed. Dittrich, A. et al.), Bundesanstalt fr Wasserbau.
1250 Schultz, M., Kozerski, H-P, Pluntke, T., Rinke, K. (2003). The influence of macrophytes on sedimentation
1251 and nutrient retention in the lower River Spree. *Water Resour. Res*., 37, 569–578.
1252 Serra, T., Fernando, H.J.S., Rodriquez, R. (2004). Effects of emergent vegetation on lateral diffusion in
1253 wetlands. *Water Research*, 38:139-47.
1254 Sharpe, R., James, C. (2006). Deposition of sediment from suspension in emergent vegetation. *Water SA*,
1255 32(2): 211-218.
1256 Siniscalchi, F., Nikora, V., Aberle, J. (2012). Plant patch hydrodynamics in streams: mean flow, turbulence,
1257 and drag forces. *Water Resour. Res*., 48, W01512, doi:10.1029/2011WR011050
1258 Shimizu, Y., Tsujimoto, T. (1994). Numerical analysis of turbulent open-channel flow over a vegetation layer
1259 using a *k-e* turbulence model. *J. Hydrosci. Hydraul. Eng*. 11:57-67.
1260 Stapleton, K., Huntley, D. (1995). Seabed stress determination using the inertial dissipation method and
1261 turbulent kinetic energy method. *Earth Surf. Process Land* 20, 807-815

1262 Statzner, B., Lamouroux, N., Nikora, V., Sagnes, P. (2006). The debate about drag and reconfiguration of
1263 freshwater macrophytes: comparing results obtained by three recently discussed approaches. *Freshwater*
1264 *Biol*. 51:2173-83.
1265 Stevens, C., Hurd, C., Isachsen. P. (2003). Modelling of diffusion boundary-layers in subtidal macrogalgal
1266 canopies: response to waves and currents. *Aquat. Sci*. 65, 81-91.
1267 Stone, B.M., Shen, H.T., (2002) Hydraulic resistance of flow in channels with cylindrical roughness. *J*
1268 *Hydraul Eng* ASCE 128(5):500–6.
1269 Sukhodolov A. (2005). Comment on drag and reconfiguration of macrophytes. *Freshwater Biol*. 50:194-95.
1270 Sukhodolova, T., Sukhodolov, A., Kozerski, H., Köhler, J. (2006). Longitudinal dispersion in a lowland river
1271 with submersed vegetation. In: River Flow 2006, Int. Conf. on Fluvial Hydr., A4021, Lisbon, Portugal.
1272 Sukhodolov, A., Sukhodolova, T. (2010). Case study: effect of submerged aquatic plants on turbulence
1273 structure in a lowland river. *J. Hydr. Eng.*, 136(7): 434-446, doi:10.1061/_ASCE_HY.1943-
1274 7900.0000195.
1275 Takemura, T., Tanaka, N. (2007), Flow structures and drag characteristics of a colony-type emergent
1276 roughness model mounted on a flat plate in uniform flow, *Fluid Dyn. Res.*, *39*, 694-710,
1277 doi:10.1016/j.fluiddyn.2007.06.001.
1278 Tal, M., Paola, C. (2007) Dynamic single-thread channels maintained by the interaction of flow and
1279 vegetation, *Geol Soc. Am*, 35:347-350.
1280 Tanino, Y., Nepf, H. (2008). Lateral dispersion in random cylinder arrays at high Reynolds number. *J. Fluid*
1281 *Mech.* 600, 339-71.
1282 Temmerman, S., Bouma, T.J., de Koppel, V., van der, W., de Vries, M.B., Herman, P.M.J. (2007), Vegetation
1283 causes channel erosion in a tidal landscape, *Geology*, *35*(7), 631–634, doi: 10.1130/G23502A.
1284 Thomas, F., Cornelisen, C. and J. Zande. (2000). Effects of water velocity and canopy morphology on
1285 ammonium uptake by seagrass communities. *Ecology* 81 (10): 2704-2713.
1286 Turker, U., Yagci, O., Kabdasli, M. (2006). Analysis of coastal damage of a beach profile under the
1287 protection of emergent vegetation. *Ocean Engineering*, 33, 810-828.
1288 US Environmental Protection Agency (2000). *Principles for the Ecological Restoration of Aquatic Resources*,
1289 Report EPA841-F-00- 003, Office of Water (4501F), Washington, DC.
1290 van Katwijk, M., Bos, A., Hermus, D., Suykerbuyk, W. (2010). Sediment modification by seagrass beds:
1291 muddification and sandification induced by plant cover and environmental conditions. *Estuar. Coast.*
1292 *Shelf Sci*., doi:10.1016/j.ecss.2010.06.008.
1293 Vereecken, H., Baetens, J., Viaene, P., Mostaert, F., Meire, P. (2006). Ecological management of aquatic
1294 plants: effects in lowland streams. *Hydrobiologia*, 570:205-210. DOI 10.1007/s10750-006-01815
1295 Velasco, D, Bateman, A., Redondo, J., Demedina, V. (2003) An open channel flow experimental and

1296 theoretical study of resistance and turbulent characterization over flexible vegetated linings. *Flow Turbul.*
1297 *Combust.* 70(1–4), 69–88.
1298 Vogel, S. (1994). *Life in Moving Fluid* 2nd ed., Princeton University Press, Princeton, NJ.
1299 Vollmer, S., Kleinhans, G. (2007). Predicting incipient motion, including the effect of turbulent pressure
1300 fluctuations in the bed. *Water Resour. Res*., 43, W05410, doi:10.1029/2006WR004919.
1301 Wang, C., Yu, J., Wang, P., Guo. P. (2009). Flow structure of partly vegetated open-channel flows with
1302 eelgrass. *J. of Hydrodynamics*, *Ser.B*., 21(3): 301-307.
1303 White, B., Nepf, H. (2007). Shear instability and coherent structures in a flow adjacent to a porous layer, *J.*
1304 *Fluid Mech*. 593:1-32.
1305 White, B., Nepf. H. (2008). A vortex-based model of velocity and shear stress in a partially vegetated shallow
1306 channel. *Water Resour. Res*., 44(1):W01412, doi. 10.1029/2006WR005651
1307 White, F.M., (2008). *Fluid Mechanics*, 6th Ed., McGraw Hill, Boston, MA, USA.
1308 Widdows, J., Pope, N., Brinsley, M. (2008). Effect of *Spartina anglica* stems on near-bed hydrodynamics,
1309 sediment erodability and morphological changes on an intertidal mudflat. *Mar. Ecol. Prog. Ser.*, 362, 45-
1310 57.
1311 Wilcock, R., Champion, P., Nagels, J., Crocker, G. (1999). The influence of aquatic macrophytes on the
1312 hydraulic and physicochemical properties of a New Zealand lowland stream, *Hydrobiologia*, **416**(1), 203-
1313 214.
1314 Windham, L., Weis, J., Weis, P. (2003). Uptake and distribution of metals in two dominant salt marsh
1315 macrophytes, *Spartina alterniflora* and *Phragmites australis*, *Estuar. Coast. Shelf Sci*., 56:63–72.
1316 Wohl, E.,Angermeier, P., Bledsoe,B.,Kondolf, G.M., Mac-Donnell, L., Merritt, D., Palmer, M., Poff, N.
1317 &Tarboton, D. (2005). River restoration. *Water Resour. Res.* 41: W10301.
1318 Wooding, R., Bradley, E., Marshall, J. (1973). Drag due to regular arrays of roughness elements. *Bound. Lay.*
1319 *Met*. 5, 285-308.
1320 Wu, F., Shen, H., Chou, Y. (1999) Variation of roughness coefficients for unsubmerged and submerged
1321 vegetation. *J Hydraul Eng* ASCE 125(9):934–42.
1322 Wynn, T., Mostaghimi, S. (2006). Effects of riparian vegetation on stream bank subaerial processes in
1323 southwestern Virginia, USA. *Earth Surf. Proc. Landforms*. 31:399-413.
1324 Zavistoski, R. (1992). Hydrodynamic Effects of Surface Piercing Plants. *SM Thesis.* Massachusetts Institute of
1325 Technology.
1326 Zimmerman, R. (2003). A biooptical model of irradiance distribution and photosynthesis in seagrass canopies,
1327 *Limnol Oceanogr* 48(1): 568-585
1328 Zong, L., Nepf. H. (2010). Flow and deposition in and around a finite patch of vegetation. *Geomorphology.*
1329 116:363-372. doi:10.1016/j.geomorph.2009.11.020.

1330 Zong, L. Nepf H. (2011). Spatial distribution of deposition within a patch of vegetation *Water Resour. Res*., 47,
1331 W03516, doi:10.1029/2010WR009516.
1332 Zong, L., Nepf. H. (2012). Vortex development behind a finite porous obstruction in a channel., *J. Fluid*
1333 *Mech*., 691: 368-391, doi:10.1017/jfm.2011.479
1334
1335